ETH
Eidgenössische Technische Hochschule Zürich
Swiss Federal Institute of Technology Zurich

Communication Technology Laboratory
Wireless Communications Group
Professor
Armin Wittneben

Master Thesis

The Use of Loaded Antennas as Scattering Relays for Post-Cellular Networks with Closely Spaced Terminals

Autumn Semester 2015

Professor: Armin Wittneben

Supervisor:
Yahia Hassan

Student:
Bernhard Gahr

Declaration of Originality

I hereby declare that the written work I have submitted entitled

Real-Time Demonstrator for ToA based Human Motion tracking System: Localization and Self-Calibration

is original work which I alone have authored and which is written in my own words.[1]

Author(s)

Bernhard	Gahr

Student supervisor(s)

Yahia	Hassan

Supervising lecturer

Armin	Wittneben

With the signature I declare that I have been informed regarding normal academic citation rules and that I have read and understood the information on 'Citation etiquette' (`https://www.ethz.ch/content/dam/ethz/associates/students/studium/exams/files-en/plagiarism-citationetiquette.pdf`). The citation conventions usual to the discipline in question here have been respected.

The above written work may be tested electronically for plagiarism.

Place and date	Signature

[1] Co-authored work: The signatures of all authors are required. Each signature attests to the originality of the entire piece of written work in its final form.

Contents

Acknowledgements

A huge project like a master thesis is never done alone, and I have many people to thank for their contributions. First, I would like to express my gratitude to my Professor Armin Wittneben for giving me the opportunity to work on this master thesis at the Wireless Communication Group.

I am also grateful to Yahia Hassan, my supervisor, for his help and guidance throughout the thesis. Yahia knew when he had to push me and when I needed a break to talk about football. I also would like to thank him for letting me be part of submitting a scientific paper, and for sharing his insights on that process.

I owe many thanks to Dr. David Adjiashvili from the institute for operation research on his help with nonconvex optimizations, and for his advice during lunch breaks. Further, I want to thank Dr. Katherine Caves for proofreading this thesis and for her advice on scientific writing, even when I was on a tight schedule.

Finally, all my love and thanks go to my family, to Laura, and to my flat mates. Mom, Dad, Martin, and Manuel, thank you for your interest in my thesis and its progress. Frederik, Philipp, and Stefan, thank you for getting my mind off the thesis when I came home. Laura, thank you for your love, and for your support during the last six months.

Abstract

In current wireless networks there are two limiting factors for transmission rates: fading and interference. While multiple-input-multiple-output (MIMO) systems reduce the impact of fading, the problem of interference has not yet been satisfyingly solved. The most common methods for addressing the problem of interference are protocols based on schemes like time-division- (TD-), frequency-division- (FD-), or code-division multiple access (CDMA). The simultaneous advantage and downfall of those schemes is their unique allocation of specific time and/or frequency slots for each user, hence blocking all other users.

In this thesis the problem of interference is addressed by using closely spaced passive relays: antennas with only passive, lossless impedances attached, which interact with the receiving antennas only through coupling. These relays require no input power to amplify signals. By using passive elements, the effects of coupling can be changed, and by using multiple passive relays couplings can be used to increase the signal and reduce the interference power to the receivers.

In the following, a description of the system will be derived that allows for an easy and elegant way of analyzing the effects of coupling. Different solver methods are analyzed and discussed in order to find the optimal choice of relay loads. As some of the solvers are based on the method of gradient search, the analytical gradient will be derived. In order to derive the analytical gradient, full channel knowledge of the spatial channel and couplings between receiving elements are assumed. For the gradient search method, a variety of initial value choices will be compared. Further, the results are evaluated and compared to different solver methods and previously known interference-limiting methods.

Notations, Acronyms and Abbreviations

Symbols

x^*	conjugate complex of x
$\mathbf{x}$	Vector
$\mathbf{x}[i]$ or $\mathbf{x}_i$	i-th element of vector $\mathbf{x}$
$\|\|\mathbf{x}\|\|_p$	P-norm of vector $\mathbf{x}$
$\mathbf{X}$	Matrix
$\mathbf{X}^T$	transpose of matrix $\mathbf{X}$
$\mathbf{X}^{-1}$	inverse of matrix $\mathbf{X}$
$\mathbf{X}^H$	hermitian transpose of matrix $\mathbf{X}$

Indices

x, y, z	x, y, z axis

Acronyms and Abbreviations

ETH	Eidgenössische Technische Hochschule
WCG	Wireless Communicatoin Group
(N)LOS	(Non) Line of Sight
ML	Maximum Likelihood
CDF	Cummulative Distribution Function
PDF	Probability Density Function
MIMO	Multiple Input Multiple Output
IoT	internet of Things
T/F/CDMA	Time/Frequency/Code Division Multiple Access
S(I/N)R	Signal to Noise/Interference Ratio
LNA	Low Noise Amplifier
N_{User}	Number of Users
N_{T}	Number of Transmitters
N_{Tx}	Number of Antennae per Transmitter
N_{R}	Number of Receiver

N_{Rx}	Number of Antennae per Receiver
N_{Relay}	Number of Relays per Receiver

List of Figures

Chapter 1

Introduction

Future wireless networks are assumed to have high receiver density, as more devices with access to the Internet appear on the market and more types of devices are staffed with modules able to connect to the Internet (Internet of things IoT) [1]. Examples of such scenarios are cellular networks in urban areas, wireless networks in public spaces like concert halls, and sensor networks.

Such networks suffer from two main rate-limiting effects: fading and interference. While the effect of fading is mostly solved by MIMO techniques, interference remains as the limiting factor for high data rates. Classical methods of overcoming interference are protocols like TDMA, FDMA, or CDMA. The downside of those protocols is their unique allocation of a user to a specific time and frequency slot, blocking of all other users. More advanced techniques use multiple antennas — similar of overcoming the problem of fading — to achieve multiple observations of the incoming signals, and therefore the ability to zero force the interfering signals. This, however, is only possible if the number of antennas per receiver is larger than the number of interfering signal streams — nearly impossible or very expensive in high-density networks as the size of the receiver structure grows rapidly [1].

In this thesis we introduce the use of passive relays, or antennas with pure imaginary impedances attached. As they are placed very close (in terms of wavelengths) around the receivers, they interact by coupling with the receivers. By the choice of loads, the strength of coupling can be changed. With an increasing number of such passive relays, couplings can be used to steer the signal towards the receiver and block interference. Full channel knowledge is assumed of the spatial channel and the coupling matrix in order to match the relay impedances.

Our strategy proved theoretically effective in situations when adapted coupling of passive relays is possible. We demonstrate that our theoretical foundation is a useful addition to previously conducted research. The paper creates new avenues for future research based on its theoretical insights.

1.1 Motivation and Goals

The achievable rate of a connection pair is dependent on the signal, noise, and interference covariance matrices. In a high power region the effect of noise can be neglected, as the interference is the main diminishing factor. Therefore an interference-free connection is the main goal.

As the method of using passive relays through only their coupling is a new way of addressing the problem of interference, this thesis will look into potential improvements rather than practical feasibility of the method. To achieve the highest possible rate for any realization, the shape of the problem is analyzed and different

solver methods are introduced and comparedS. Maximum achievable rates shall be given for different settings and topologies in order to enable judgment of which settings for with this method is suitable.

1.2 State of the Art

Six papers are key to current solutions for interference in large multi-user systems. [1] discovered that transmission rates decrease in the presence of large numbers of antennas. [2] described the problem connecting information theory and circuit theory, contributing a novel and useful description of large systems using circuit theory. Following up on that work, [3] used gradient search to optimize large networks—we follow that approach. Using relays, [4] were able eliminate interference. [5] steered antenna beams toward the intended target using relays. Finally, [6] used relays to uncouple antennas. We build upon all of these approaches in this paper.

Because interference is a main problem in larger multi user systems, effects of largely scaled MIMO systems must be studied.

In [1] F. Rusek et al. wrote about scaling up MIMO systems. They exploit opportunities and challenges of large systems with hundreds of antennas. Among other things, they look into the mutual coupling and spatial correlation of large antenna arrays at the transmitter. They came to the conclusion that interactions among antenna elements can incur significant losses, because for large MIMO systems the antenna spacing becomes smaller. Therefore it is important to analyze the behavior of closely spaced antennas.

Working with closely spaced antenna elements requires a useful way of describing couplings. In [2] M. Ivrlac et al. describe compact systems using circuit theory. Their description is also usable for this thesis with some adaptation. Additionally they find an optimal setting for the matching network on the receiver side, called multi-port matching. Multi-port matching will be used in this thesis to serve as theoretical upper limit. For large antenna systems, multi-port matching becomes very complex, and hence hard to implement. Therefore, this thesis looks into a different approach to optimize the achievable rate.

Further research on the matching network was done in [3]. A gradient-search algorithm is developed to design a matching network for achievable rate maximization of multi-user MIMO systems. Their settings are adapted for this thesis. Additionally, we improved upon their developments by using passive relays to amplify the signal and reduce the interference at the receiver.

Although only TDMA has been mentioned so far, further approaches on interference elimination methods exist. In [4], the concept of Distributive Spatial Multiplexing (DSM), is introduced. This attempts to eliminate interference by using amplify and forward (AF) relays. By choosing different amplify gains for each relay, the interference can be eliminated at each receiver. In contrast to the approach in this thesis, their relays are not lossless and require a power source to amplify their signals.

Further research on passive relays, or parasitic elements was done in [5]. They use these parasitic elements to steer the receiving antenna beam. However, for more closely spaced transmitters or signals with a similar angle of incidence, this will not eliminate any interference. We also use passive relays, but in a different context.

Finally, two antennas were uncoupled from each other in [6] by placing parasitic elements in the middle. For an orthogonal channel this will remove the interference. If however — as it is in this thesis — a spatial interference channel is assumed, both receivers will collect an interfering signal. Therefore this thesis tries to use the coupling itself to reduce interference, instead of trying to uncouple the receivers from each other.

Building on all of this work, we address the problem of interference in scaled-up MIMO systems from a circuit theory perspective. We add to this by incorporating information theory, forging a connection between the two. In our implementation we follow the guidance of other studies and use passive relays and the effect of coupling to design a novel method for reducing interference and amplifying the signal.

1.3 Outline

In the following chapter the whole system is described by connecting circuit theory and information theory. The effect of coupling is analyzed and the overall transfer function — from the transmitter to the receiver — is stated. A description of the spatially correlated interference channel is given. All the noise sources appearing in the systems and their transfer function are shown and derived. The transfer functions are split up into smaller, simpler subfunctions, such that the effect of coupling and the interference can be better described and analyzed.

As one of the optimization methods is gradient search, in the third chapter the analytical gradients are derived — for the signal, the interference and the noise. The gradient is dependent on the covariance matrix, therefore they are derived as well for the signal, interference, and noise contributions at the receiver.

In the fourth chapter, different optimization methods are introduced and compared to each other. Aside from the method of gradient search, there are heuristic algorithms introduced. Further improvements in precision and speed of the optimization methods performance are introduced.

The results of the optimization methods and their improvements are evaluated in the fifth chapter. The results is compared to different numbers of relays used in a setup, different relay placements, and different numbers of users. Additionally, theoretical limits of the setups are derived and shown, and the results are compared to current protocols for overcoming interference, such as TDMA.

Finally, in the sixth chapter, a summary of the work achieved in this thesis and an outlook for possible future work is given.

Chapter 2

System Description

In the following, we describe the system. Figure 2.1 gives an overview. The transmitters on the left are assumed to be widely spaced, so that they experience no coupling between themselves. The signals are transmitted over a spatial interference channel such that seach signal reaches every receiver.

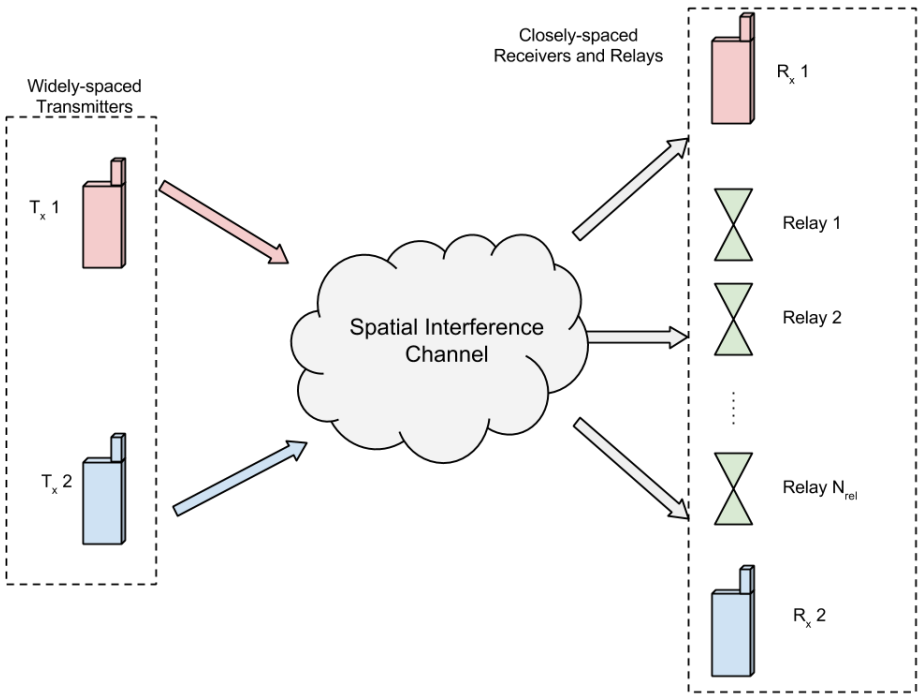

Figure 2.1: Overview of the system.

In addition to the receivers themselves, there are passive relays on the right side. The relays and receivers are closely spaced, therefore the channels between transmitters, receivers and relays are spatially correlated and the elements on the receiver side experience coupling among themselves.

2.1 Spatial Channel

As mentioned in the previous section the spatial channel is generated by spatial correlation among the receivers and the relays, dependent on the distance. The correlation matrix is generated by the Besselfuntion according to

$$R_{i,j} = J_0\left(2 \cdot \pi \cdot \frac{d_{i,j}}{\lambda}\right), \tag{2.1}$$

where $J_0(x)$ is the 0-th Besselfunction [7, p.191] and $d_{i,j}$ the distance between receiving element i and j (receiving antennas and relays are concatenated). Therefore $\mathbf{R}$ is symmetric with 1 on its diagonal, as $J_0(0) = 1$.

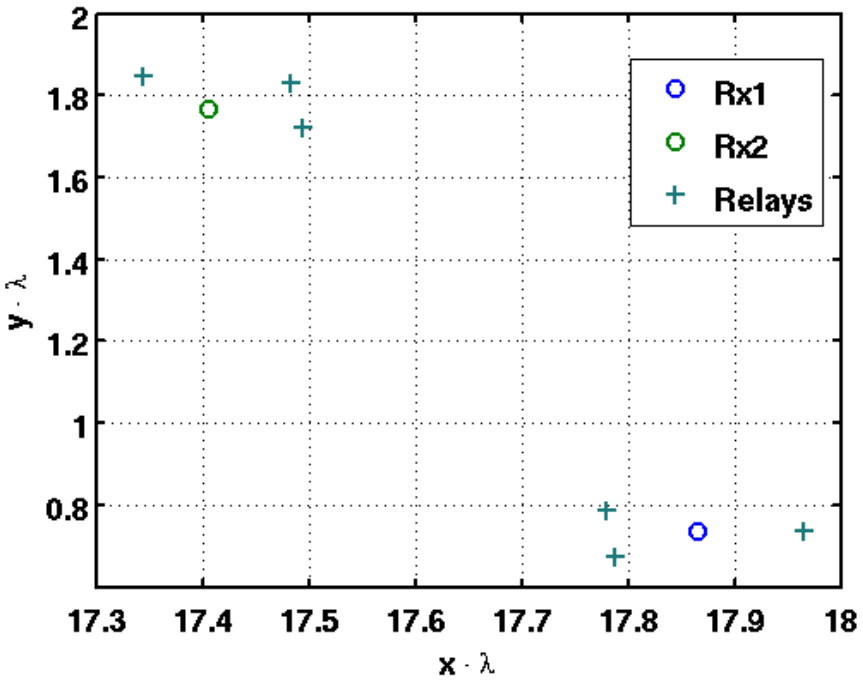

Figure 2.2: Example of the receive antenna and the relay placing.

The spatial channel from the n-th transmitter to all receivers an relays is then generated by

$$\mathbf{H}_n^{\text{sp}} = \mathbf{R}^{\frac{1}{2}} \cdot \mathbf{H}_{\text{IID}}, \tag{2.2}$$

where $\mathbf{H}_{\text{IID}}$ is a matrix of size $\mathbb{C}^{N_{\text{R}} \cdot (N_{\text{Rx}} + N_{\text{Rel}}) \times N_{\text{Tx}}}$, with complex elements drawn from the standard normal distribution ($\mu = 0$ and $\sigma = 1$). Therefore $\mathbf{H}_n^{\text{sp}}$ is of size $\mathbb{C}^{N_{\text{R}} \cdot (N_{\text{Rx}} + N_{\text{Rel}}) \times N_{\text{Tx}}}$.

2.2 Receiver Circuit Description

As mentioned in Section 1.2, the idea of describing receiver circuitry is based on the work of [2]. To do so, we represent each receiver block (shown in Figure 2.4) using n-ports. A short overview on two-ports (simplified n-ports) is given in the following.

2.2.1 Multi-Port Networks

This section starts with an analysis of a two-port network. Later, this can be easily extended to a multi-port, or n-port network.

Figure 2.3: A two-port network [8].

Figure 2.3 shows a two-port network. The two-port network can be represented by an impedance matrix $\mathbf{Z}$. The elements Z_{ij} of the matrix are defined in the following way:

$$Z_{ij} = \frac{V_i}{I_j}, \quad \text{for the currents} \quad I_l = 0, \quad l \neq j. \tag{2.3}$$

Therefore the two-port's input/output relations can be written as

$$\begin{bmatrix} V_1 \\ V_2 \end{bmatrix} = \mathbf{Z} \cdot \begin{bmatrix} I_1 \\ I_2 \end{bmatrix} \tag{2.4}$$

For a n-port network, the voltage and current elements can be represented as vectors on length n, and the elements $Z_{ij}, \quad i,j \in \{1,2\}$ become sub-matrices. Looking from the left into the network with loads R_L attached to the ports on the right, the equivalent input impedance matrix becomes

$$\mathbf{Z}_{\mathrm{eq}_1} = \mathbf{Z}_{11} - \mathbf{Z}_{21} \cdot (\mathbf{Z}_{22} + R_L \cdot \mathbf{I})^{-1} \cdot \mathbf{Z}_{12}. \tag{2.5}$$

With no load attached on port two (open circuited ports, or $R_L \to \infty$), the equivalent input impedance becomes

$$\mathbf{Z}_{\mathrm{eq}_1} = \mathbf{Z}_{11}. \tag{2.6}$$

Last, having port one short-circuited (i.e. $R_L \to 0$) and looking from port two into the network, the equivalent network impedance becomes

$$\mathbf{Z}_{\mathrm{eq}_2} = \mathbf{Z}_{22} - \mathbf{Z}_{12} \cdot (\mathbf{Z}_{11})^{-1} \cdot \mathbf{Z}_{21}. \tag{2.7}$$

For reciprocal networks (RLC-Networks, containing only passive elements), the following property holds: $\mathbf{Z}_{12} = \mathbf{Z}_{21}^T$.

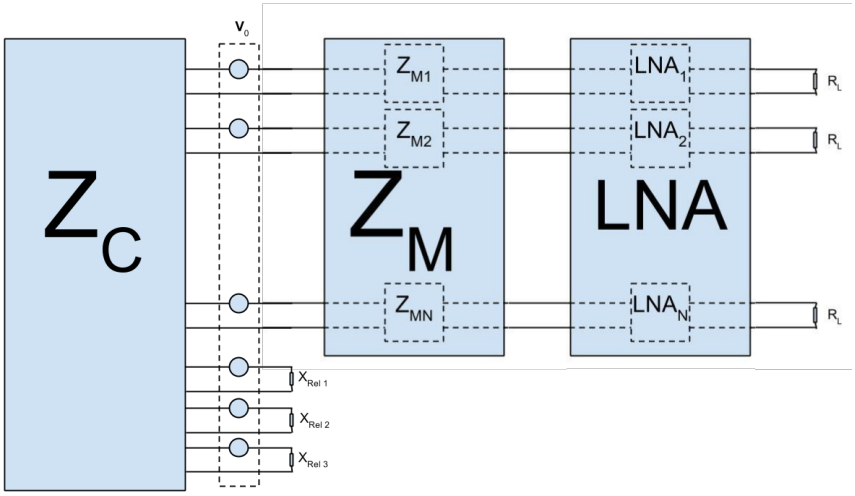

Figure 2.4: The receiver, with the coupling network $\mathbf{Z}_\mathrm{C}$, the SP-matching network $\mathbf{Z}_\mathrm{M}$, the LNA, and loads attached to the LNA.

2.2.2 Receiver Blocks

The receiver (as shown in Figure 2.4) consists of three blocks. From left to right:

1. the coupling network ($\mathbf{Z}_\mathrm{C}$),
2. the matching network ($\mathbf{Z}_\mathrm{M}$), and
3. the low-noise-amplifier (**LNA**).

All of these blocks can be described as multi-port networks. In the following each block is discussed.

The Coupling Network

The coupling network is introduced, as a compact antenna spacing is assumed on the receiver side. The strength of the coupling between two antennas depends on the type of the antennas and the spacing between themselves. We model the antennas as half wavelength dipoles. As the effect of coupling from one antenna to another is the same as the reverse, the impedance matrix $\mathbf{Z}_\mathrm{C}$ becomes symmetric. Coupling among antennas is calculated by the "EWA"-Toolbox for MATLAB [9]. The theory underlying this can be found in [9, Chapter 23].

The Matching Network

In order to improve the performance of the receiver, a matching network is placed after each receiving antenna. For complexity and bandwidth reasons, single-port (SP) matching is assumed [3]. The matching network has the form of

$$\mathbf{Z}_\mathrm{M} = \begin{bmatrix} \mathbf{Z}_\mathrm{M11} & \mathbf{Z}_\mathrm{M12} \\ \mathbf{Z}_\mathrm{M21} & \mathbf{Z}_\mathrm{M22} \end{bmatrix}. \tag{2.8}$$

For a matching network to be lossless, it must be purely imaginary and symmetric [2]. Because we assume SP matching, the sub-matrices become diagonal. With the choice of a reciprocal network, additionally following property holds: $\mathbf{Z}_\mathrm{M12} = \mathbf{Z}_\mathrm{M21}^T \implies \mathbf{Z}_\mathrm{M12} = \mathbf{Z}_\mathrm{M21}$. Further, the network can be represented as a T-network, which is shown in Figure 2.5.

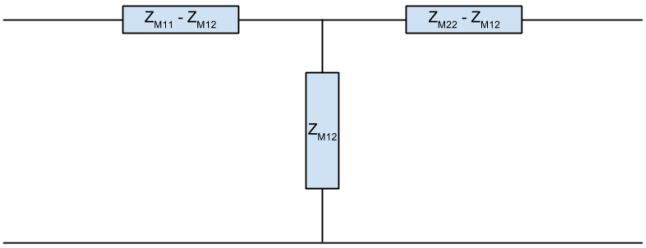

Figure 2.5: Schematic of a reciprocal T-network.

The Low-Noise-Amplifier

In the LNA block the received signal is amplified after the matching network. As in the matching network, the LNA can be represented in the following way

$$\mathbf{LNA} = \begin{bmatrix} \mathbf{c} & \mathbf{d} \\ \mathbf{e} & \mathbf{g} \end{bmatrix}. \tag{2.9}$$

As each branch has its own LNA, the sub-matrices $\mathbf{c}, \mathbf{e}$, and $\mathbf{g}$ are again diagonal. Additionally, matrix $\mathbf{d}$ is an all-zeros matrix under the unilateral assumption (*the input of the LNA is not affected by the output of the LNA*).

2.2.3 Port Reduction

In the following, we describe the open circuit reduction of a system like that in Figure 2.6. We perform port reduction because we are interested in the signal only at the loads of the corresponding receiver. The signal picked up at relay antennae or receivers not considered contributes to the signal at the considered receiver through the coupling between the antennas, as described in Section 2.2.2. The passive relays are modeled by connecting an impedance directly to the coupling network as shown in the lowest two branches on the left in Figure 2.6. Undesired receivers can be modeled in the same manners as the relays, with the load corresponding to the equivalent input impedance of the matching network (as in Equation (2.17)) shown by the third lowest branch on the left in Figure 2.6.

In the following, $\mathbf{v}_{\mathrm{C}i}$ denotes the parallel voltages on the ports at the coupling matrix $\mathbf{Z}_{\mathrm{C}}$ and $\mathbf{i}_{\mathrm{C}i}$ denotes the same for the currents. As we are not interested in the input/output relationships between these passive antennas, a port reduction is performed. For the port reduction, the coupling matrix $\mathbf{Z}_{\mathrm{C}}$ can be represented by four sub-matrices

$$\mathbf{Z}_{\mathrm{C}} = \begin{bmatrix} \mathbf{Z}_{\mathrm{OO}} & \mathbf{Z}_{\mathrm{OL}} \\ \mathbf{Z}_{\mathrm{LO}} & \mathbf{Z}_{\mathrm{LL}} \end{bmatrix}, \tag{2.10}$$

so that we get the system relations

$$\begin{bmatrix} \mathbf{v}_{\mathrm{CO}} \\ \mathbf{v}_{\mathrm{CL}} \end{bmatrix} = \begin{bmatrix} \mathbf{Z}_{\mathrm{OO}} & \mathbf{Z}_{\mathrm{OL}} \\ \mathbf{Z}_{\mathrm{LO}} & \mathbf{Z}_{\mathrm{LL}} \end{bmatrix} \cdot \begin{bmatrix} \mathbf{i}_{\mathrm{CO}} \\ \mathbf{i}_{\mathrm{CL}} \end{bmatrix}. \tag{2.11}$$

The index O denotes the ports of the required receiver branches, which are open-circuited, the index L represents ports of the non-required receivers and the relays (i.e. the ports with an impedance attached or loaded, respectively). Therefore, $\mathbf{Z}_{\mathrm{OO}}$ is of size $\mathbb{C}^{N_{\mathrm{Rx}} \times N_{\mathrm{Rx}}}$, $\mathbf{Z}_{\mathrm{OL}}$ of size $\mathbb{C}^{N_{\mathrm{Rx}} \times N_{\mathrm{R}} \cdot (N_{\mathrm{Rx}} + N_{\mathrm{Rel}})}$, and $\mathbf{Z}_{\mathrm{LL}}$ of size $\mathbb{C}^{N_{\mathrm{R}} \cdot (N_{\mathrm{Rx}} + N_{\mathrm{Rel}}) \times N_{\mathrm{R}} \cdot (N_{\mathrm{Rx}} + N_{\mathrm{Rel}})}$. The indices will change depending on the user. Without loss of generality, we will derive the port reduction only for the first receiver (receiver 0 in the following. We assume that there are $N_{\mathrm{R}} \cdot N_{\mathrm{Rx}}$ antennas, whereof

the first N_{Rx} antennas are active (i.e. are the receive antenna of user 0) and the later ones are passive (i.e. the antennas of the relays and of the other users). $\mathbf{Z}_{\text{pass}}$ denotes in the following the $(N_{\text{R}}-1)\cdot N_{\text{Rx}}$ equivalent input impedances $\mathbf{Z}_{\text{eqM1}}$ of the non-required receivers and the N_{Rel} impedances representing the relays $\mathbf{X}_{\text{Rel}}$, placed on the diagonal of a $\mathbb{C}^{(N_{\text{R}}-1)\cdot N_{\text{Rx}}+N_{\text{R}}N_{\text{Rel}}\times(N_{\text{R}}-1)\cdot N_{\text{Rx}}+N_{\text{R}}N_{\text{Rel}}}$ square matrix.

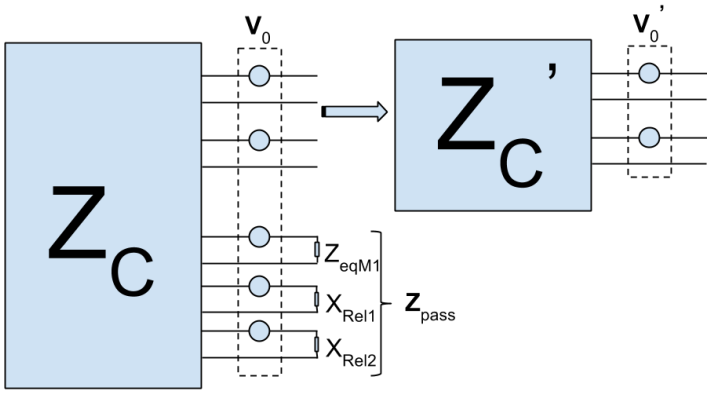

Figure 2.6: Port reduction on a network with one load connected to the last port.

From Equation (2.11) and the property

$$\mathbf{v}_{\text{CL}} = \mathbf{v}_O[N_{Rx}+1 : N_R \cdot N_{Rx}] - \mathbf{Z}_{\text{pass}} \cdot \mathbf{i}_{\text{CL}} \tag{2.12}$$

it follows that

$$\begin{aligned}\mathbf{i}_{\text{CL}} = &-(\mathbf{Z}_{\text{pass}} + \mathbf{Z}_{\text{LL}})^{-1}\mathbf{Z}_{\text{LO}} \cdot \mathbf{i}_{\text{CO}} - \\ &(\mathbf{Z}_{\text{pass}} + \mathbf{Z}_{\text{LL}})^{-1} \cdot \mathbf{v}_0[N_i+1 : N_R]\end{aligned} \tag{2.13}$$

and therefore,

$$\begin{aligned}\mathbf{v}_{\text{CO}} = &(\mathbf{Z}_{\text{OO}} - \mathbf{Z}_{\text{OL}}(\mathbf{Z}_{\text{pass}} + \mathbf{Z}_{\text{LL}})^{-1}\mathbf{Z}_{\text{LO}}) \cdot \mathbf{i}_{\text{CO}} - \\ &\mathbf{Z}_{\text{OL}}(\mathbf{Z}_{\text{pass}} + \mathbf{Z}_{\text{LL}})^{-1} \cdot \mathbf{v}_0[N_{Rx}+1 : N_R \cdot N_{Rx}].\end{aligned} \tag{2.14}$$

With this port reduction, the equivalent coupling matrix $\mathbf{Z}_{\text{C}}^{'}$ and input voltage $\mathbf{v}_0^{'}$ for receiver 0 become

$$\mathbf{Z}_{\text{C}}^{'} = \mathbf{Z}_{\text{OO}} - \mathbf{Z}_{\text{OL}}(\mathbf{Z}_{\text{pass}} + \mathbf{Z}_{\text{LL}})^{-1}\mathbf{Z}_{\text{LO}} \quad \text{and} \tag{2.15}$$

$$\begin{aligned}&\mathbf{v}_0^{'} = \mathbf{H}_0^{\text{pr}} \cdot \mathbf{H}_j^{\text{sp}} \cdot \mathbf{v}_j, \\ &\text{with} \quad \mathbf{H}_0^{\text{pr}} = \left[\mathbf{I}_{N_{\text{Rx}}} \quad -\mathbf{Z}_{\text{OL}}(\mathbf{Z}_{\text{pass}} + \mathbf{Z}_{\text{LL}})^{-1}\right],\end{aligned} \tag{2.16}$$

for any transmitter j, with $j \in \{0, ..., N_{\text{T}}-1\}$. It is easy to see that $\mathbf{Z}_{\text{C}}^{'}$ has size $\mathbb{C}^{N_{\text{Rx}}\times N_{\text{Rx}}}$. Further, $\mathbf{v}_0^{'}$ is of length $\mathbb{C}^{N_{\text{Rx}}\times 1}$, as $\mathbf{H}_0^{\text{pr}}$ is of size $\mathbb{C}^{N_{\text{Rx}}\times N_{\text{R}}\cdot(N_{\text{Rx}}+N_{\text{Rel}})}$ and $\mathbf{H}_j^{\text{sp}}$ has size $\mathbb{C}^{N_{\text{R}}\cdot(N_{\text{Rx}}+N_{\text{Rel}})\times N_{\text{T}}N_{\text{Tx}}}$. Therefore we can reduce the system shown in Figure 2.4, to a simpler system, which only considers the branches of the receiving antenna.

2.2.4 Transfer Function of the Receiver

Our main interest lies in the transfer function $\mathbf{H}_{\text{L},i}$ of the input voltages $\mathbf{H}_j^{\text{sp}} \cdot \mathbf{v}_{\text{j}}$ to the voltage measured at the loads (in Figure 2.4) $\mathbf{v}_{\text{L},i}$. In this the signal is transmitted by user j and received by user i.

In the following the transfer function for each block of the receiver is derived. We use the following terminology: $\mathbf{v}_l$ are the voltages on the left of the block l (e.g. $\mathbf{v}_\mathrm{M}$ are the voltages on the left ports of the matching network). Also, for simplicity reasons the index of the receiver blocks corresponding to the user i. Additionally, we see the left ports as input ports and the right ports as output ports for each block. We need four equivalent impedance matrices for the derivation of the transfer function, namely:

1. $\mathbf{Z}_\mathrm{eqM1}$, the impedance matrix looking from the left into the matching network,
2. $\mathbf{Z}_\mathrm{eqM2}$, the impedance matrix looking from the right into the matching network,
3. $\mathbf{Z}_\mathrm{eqLNA1}$, the impedance matrix looking from the left into the LNA, and
4. $\mathbf{Z}_\mathrm{eqLNA2}$, the impedance matrix looking from the right into the LNA.

To calculate $\mathbf{Z}_\mathrm{eqM1}$ and $\mathbf{Z}_\mathrm{eqLNA1}$, we use Equation (2.5) and the unilateral assumption ($\mathbf{d} = 0$) to find

$$\mathbf{Z}_\mathrm{eqM1} = \mathbf{Z}_\mathrm{M11} - \mathbf{Z}_\mathrm{M21} \cdot (\mathbf{Z}_\mathrm{M22} + \mathbf{Z}_\mathrm{eqLNA1})^{-1} \cdot \mathbf{Z}_\mathrm{M12}, \quad \text{and} \tag{2.17}$$

$$\mathbf{Z}_\mathrm{eqLNA1} = \mathbf{c} - \mathbf{e} \cdot (R_L \mathbf{I}_{N_R} + \mathbf{g})^{-1} \cdot \mathbf{d} = \mathbf{c}. \tag{2.18}$$

For our calculations we assume that port reduction has been performed on the system. Hence, the sub-matrices of the matching network and the LNA — and therefore also the equivalent input impedance matrices — are of size $\mathbb{C}^{N_\mathrm{Rx} \times N_\mathrm{Rx}}$.

As we step through the receiver blocks from left to right, we always apply the parallel voltages to each receiver block on the left. Therefore, the equivalent input impedances $\mathbf{Z}_\mathrm{eqM2}$ and $\mathbf{Z}_\mathrm{eqLNA2}$ can be derived using the unilateral assumption again and Equation (2.6), which leads to:

$$\mathbf{Z}_\mathrm{eqM2} = \mathbf{Z}_\mathrm{M22} - \mathbf{Z}_\mathrm{M12} \cdot (\mathbf{Z}_\mathrm{M11})^{-1} \cdot \mathbf{Z}_\mathrm{M21}, \quad \text{and} \tag{2.19}$$

$$\mathbf{Z}_\mathrm{eqLNA2} = \mathbf{g} - \mathbf{d} \cdot (\mathbf{c})^{-1} \cdot \mathbf{e} = \mathbf{g}. \tag{2.20}$$

To attain the parallel input voltages on the left of the matching network, we use the principle of a voltage divider, which is

$$\mathbf{v}_\mathrm{M} = \mathbf{Z}_\mathrm{eqM1} \cdot (\mathbf{Z}_\mathrm{eqM1} + \mathbf{Z}_\mathrm{C})^{-1} \mathbf{H}_i^\mathrm{pr} \cdot \mathbf{H}_j^\mathrm{sp} \cdot \mathbf{v_j}. \tag{2.21}$$

To transfer the voltages from the left ports to the right ports of each block, we proceed for each block in the following manner:

1. Calculate the input currents,
2. Transfer the input currents to the output voltages in series, and
3. Calculate the output voltages in parallel using a voltage divider.

For the matching network, it follows that:

$$\mathbf{i_M} = \mathbf{Z}_\mathrm{M11}^{-1} \cdot \mathbf{v}_\mathrm{M}, \tag{2.22}$$

$$\mathbf{v}_{\mathrm{LNA}_\mathrm{series}} = \mathbf{Z}_\mathrm{M12} \cdot \mathbf{i_M} = \mathbf{Z}_\mathrm{M12} \mathbf{Z}_\mathrm{M11}^{-1} \cdot \mathbf{v}_\mathrm{M}, \tag{2.23}$$

$$\begin{aligned} \mathbf{v}_\mathrm{LNA} &= \mathbf{Z}_\mathrm{eqLNA1} (\mathbf{Z}_\mathrm{eqLNA1} + \mathbf{Z}_\mathrm{eqM2})^{-1} \cdot \mathbf{v}_{\mathrm{LNA}_\mathrm{series}} \\ &= \mathbf{Z}_\mathrm{eqLNA1} (\mathbf{Z}_\mathrm{eqLNA1} + \mathbf{Z}_\mathrm{eqM2})^{-1} \mathbf{Z}_\mathrm{M12} \mathbf{Z}_\mathrm{M11}^{-1} \cdot \mathbf{v}_\mathrm{M}, \end{aligned} \tag{2.24}$$

and equivalently for the LNA block:

$$\mathbf{v_L} = R_L \mathbf{I}_{N_\mathrm{Rx}} (R_L \mathbf{I}_{N_\mathrm{Rx}} + \mathbf{Z}_\mathrm{eqLNA2})^{-1} \mathbf{e} \cdot \mathbf{c}^{-1} \cdot \mathbf{v}_\mathrm{LNA}. \tag{2.25}$$

Therefore we have four sub-transfer functions in total, including the port reduction transfer function, to describe the receiver side. Denoting the transfer function form voltage $\mathbf{v}_j$ to voltage $\mathbf{v}_i$ as $\mathbf{H}_{i,j}$ (i.e. $\mathbf{v}_i = \mathbf{H}_{i,j} \cdot \mathbf{v}_j$), it follows that

$$\mathbf{H}_{\mathrm{M,O'}} = \mathbf{Z}_{\mathrm{eqM1}} \cdot (\mathbf{Z}_{\mathrm{eqM1}} + \mathbf{Z}_{\mathrm{C}}^{'})^{-1}, \tag{2.26}$$

$$\mathbf{H}_{\mathrm{LNA,M}} = \mathbf{Z}_{\mathrm{eqLNA1}}(\mathbf{Z}_{\mathrm{eqLNA1}} + \mathbf{Z}_{\mathrm{eqM2}})^{-1}\mathbf{Z}_{\mathrm{M12}}\mathbf{Z}_{\mathrm{M11}}^{-1}, \quad \text{and} \tag{2.27}$$

$$\mathbf{H}_{\mathrm{L,LNA}} = R_L\mathbf{I}_{N_{\mathrm{Rx}}}(R_L\mathbf{I}_{N_{\mathrm{Rx}}} + \mathbf{Z}_{\mathrm{eqLNA2}})^{-1}\mathbf{e} \cdot \mathbf{c}^{-1}, \tag{2.28}$$

and therefore the overall transfer function is

$$\mathbf{H}_{\mathrm{L},i} = \mathbf{H}_{\mathrm{L,LNA}} \cdot \mathbf{H}_{\mathrm{LNA,M}} \cdot \mathbf{H}_{\mathrm{M,O'}} \cdot \mathbf{H}_i^{\mathrm{pr}}, \tag{2.29}$$

including a port reduction towards receiver i. As the first three sub-transfer functions ($\mathbf{H}_{\mathrm{L,LNA}}$, $\mathbf{H}_{\mathrm{LNA,M}}$ and $\mathbf{H}_{\mathrm{M,0'}}$) are of size $\mathbb{C}^{N_{\mathrm{Rx}} \times N_{\mathrm{Rx}}}$, the overall transfer function is of size $\mathbb{C}^{N_{\mathrm{Rx}} \times N_{\mathrm{R}} \cdot (N_{\mathrm{Rx}} + N_{\mathrm{Rel}})}$.

2.2.5 Signal Covariance Matrix

To calculate the achievable sum rate of the systems (c.f. Section 2.4), we need to derive the signal covariance matrix, defined as $\mathbb{E}[\mathbf{v}_{\mathrm{L},i}^s \mathbf{v}_{\mathrm{L},i}^{s^H}]$.

The overall transfer functions from $\mathbf{v}_i$ to $\mathbf{v}_{\mathrm{L},i}^s$ can therefore be extended from Equation (2.29) to

$$\begin{aligned} \mathbf{v}_{\mathrm{L},i} &= \mathbf{H}_{\mathrm{L,LNA}} \cdot \mathbf{H}_{\mathrm{LNA,M}} \cdot \mathbf{H}_{\mathrm{M,O'}} \cdot \mathbf{H}_i^{\mathrm{pr}} \cdot \mathbf{H}_i^{\mathrm{sp}} \cdot \mathbf{v}_i \\ &= \mathbf{H}_{\mathrm{L},i} \cdot \mathbf{H}_i^{\mathrm{sp}} \cdot \mathbf{v}_i, \end{aligned} \tag{2.30}$$

and the signal covariance matrix then becomes

$$\mathbf{K}_{\mathrm{S},i} = \mathbf{H}_{\mathrm{L,i}} \cdot \mathbf{H}_i^{\mathrm{sp}} \cdot \mathbb{E}[\mathbf{v}_i \mathbf{v}_i^H] \cdot \mathbf{H}_i^{\mathrm{sp}^H} \cdot \mathbf{H}_{\mathrm{L,i}}^H, \tag{2.31}$$

where $\mathbf{H}_{\mathrm{L,i}}$ is the transfer function including any port reduction at the receiver derived in Equation (2.29) and $\mathbf{H}_i^{\mathrm{sp}}$ is the transfer function over the spatial channel derived in Equation (2.2).

2.2.6 Interference Covariance Matrix

To calculate the interference covariance matrix, all of the signal sources aside from the partner (in this case, all but i) must be considered. This means that all signal elements arriving at the loads of receiver i must be summed up over all interferers. The interference covariance matrix becomes

$$\begin{aligned} \mathbf{K}_{\mathrm{I},i} &= \sum_{j=0, j\neq i}^{N_{\mathrm{User}}-1} \mathbf{H}_{\mathrm{L,i}} \cdot \mathbf{H}_j^{\mathrm{sp}} \cdot \mathbb{E}[\mathbf{v}_j \mathbf{v}_j^H] \cdot \mathbf{H}_j^{\mathrm{sp}^H} \cdot \mathbf{H}_{\mathrm{L,i}}^H \\ &= \mathbf{H}_{\mathrm{L,i}} \cdot \left(\sum_{j=1, j\neq i}^{N_{\mathrm{User}}-1} \mathbf{H}_j^{\mathrm{sp}} \cdot \mathbb{E}[\mathbf{v}_j \mathbf{v}_j^H] \cdot \mathbf{H}_j^{\mathrm{sp}^H} \right) \cdot \mathbf{H}_{\mathrm{L,i}}^H. \end{aligned} \tag{2.32}$$

2.3 Noise Description

As mentioned in [3], there are four main noise sources in the receiver. In the following, each noise source is described and its transfer function towards the loads is derived.

Figure 2.7 gives an overview of the different noise sources. It is important to note, that the first three noise sources ($\mathbf{n}_{\mathrm{AR}}$, $\mathbf{v}_{\mathrm{LNA}}$ and $\mathbf{i}_{\mathrm{LNA}}$) also contribute to the other

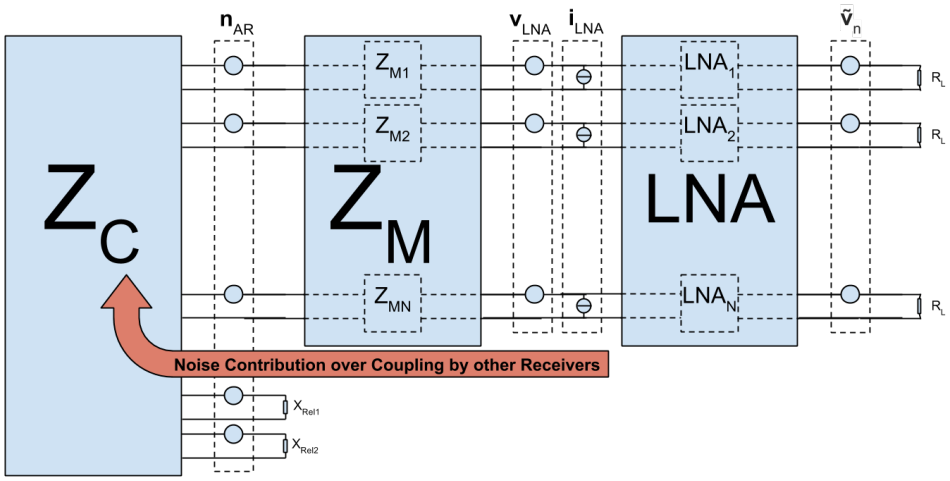

Figure 2.7: Overview of the system including noise sources.

receivers through coupling. Only the downstream noise $\tilde{\mathbf{v}}_n$ contributes exclusively to its own receiver because of the unilateral assumption of the LNA.

In the following, the transfer functions for the different noise sources are derived, such that in the end, the total noise contribution at the receiver can be expressed as

$$\begin{aligned}\mathbf{u}_{\mathrm{L}} &= \mathbf{u}_{\mathrm{AR}} + \mathbf{u}_{\mathrm{LNA}_v} + \mathbf{u}_{\mathrm{LNA}_c} + \mathbf{u}_{\tilde{n}}, \\ &= f(\mathbf{n}_{\mathrm{AR}}) + g(\mathbf{v}_{\mathrm{LNA}}) + h(\mathbf{i}_{\mathrm{LNA}}) + k(\tilde{\mathbf{v}}_{\mathrm{n}}),\end{aligned} \tag{2.33}$$

with f, g, h, and k as the transfer functions for each noise source.

2.3.1 Antenna Noise

The antennas introduce two noise sources. The external noise $\mathbf{n}_{\mathrm{ext}}$, is collected from the radiation component of the antenna array and the noise generated by the losses in the antennas $\mathbf{n}_l$. From [10] it follows that

$$\mathbf{R}_{\mathrm{na}} = \mathbb{E}[\mathbf{n}_{\mathrm{AR}}\mathbf{n}_{\mathrm{AR}}^H] = 4k_B B_W (T_{\mathrm{AE}}\mathbb{R}\{\mathbf{Z}_{\mathrm{AR}}\} + T_{\mathrm{AL}}\mathbf{R}_{\mathrm{AR}}), \tag{2.34}$$

with k_B the Boltzmann constant and B_W the bandwidth.

Transfer Function of the Antenna Noise

As the antenna noise is picked up by the antennas in the same way as the signal, the transfer function remains the same as that derived in Equation (2.30) for the signal:

$$\mathbf{H}_{\mathrm{L,i}} = \mathbf{H}_{\mathrm{L,LNA}} \cdot \mathbf{H}_{\mathrm{LNA,M}} \cdot \mathbf{H}_{\mathrm{M,O'}} \cdot \mathbf{H}_i^{\mathrm{pr}}. \tag{2.35}$$

2.3.2 LNA Noise

The LNA introduces the third noise source. Based on the discussion in [2], the noise of the LNA is modeled as a series of voltages and parallel currents at the input of

the LNA Block. The noise sources have the following statistical properties,

$$\begin{aligned} \mathbb{E}[\mathbf{i}_{\mathrm{LNA}}\mathbf{i}_{\mathrm{LNA}}^H] &= \beta \cdot \mathbf{I}_{N_{\mathrm{R}}N_{\mathrm{Rx}}}, \\ \mathbb{E}[\mathbf{v}_{\mathrm{LNA}}\mathbf{v}_{\mathrm{LNA}}^H] &= \beta \cdot R_n^2\mathbf{I}_{N_{\mathrm{R}}N_{\mathrm{Rx}}}, \quad \text{and} \\ \mathbb{E}[\mathbf{v}_{\mathrm{LNA}}\mathbf{i}_{\mathrm{LNA}}^H] &= \rho\beta \cdot R_n\mathbf{I}_{N_{\mathrm{R}}N_{\mathrm{Rx}}}, \end{aligned} \tag{2.36}$$

with ρ and β as correlation coefficients.

Transfer Function of the LNA Noise

As written above, we have two noise sources: the serial voltage sources and the parallel current sources. For each of them we must consider that the loads have noise contributions from the LNA of their own receiver branches and LNA noise from the other receiver branches through coupling. Therefore, two transfer functions are derived in the following:

1. Indirect — a transfer function towards the antenna — and
2. Direct — a transfer function towards the loads.

With the indirect transfer function derived, we can (as in the previous section) concatenate the transfer function of the signal to get the LNA noise contributions of the other receivers.

Direct LNA Noise Contribution: First, we transfer the current source into a voltage source in series. We then can use the same transfer function for the voltage and the transferred current sources. To do so, we need the equivalent input impedances looking from the left into the LNA block and from the right into the matching network. The equivalent input impedance for the LNA network $\mathbf{Z}_{\mathrm{eqLNA_1}}$ was already derived in (2.18). To get the equivalent input impedance for the matching network looking from the right, we use Equation (2.5) and find

$$\tilde{\mathbf{Z}}_{\mathrm{eqM_2}} = \mathbf{Z}_{\mathrm{M22}} - \mathbf{Z}_{\mathrm{M12}} \cdot (\mathbf{Z}_{\mathrm{M11}} + \mathbf{Z}_{\mathrm{C'}})^{-1} \cdot \mathbf{Z}_{\mathrm{M21}}. \tag{2.37}$$

Transferring the current source into a series of voltages gives us

$$\mathbf{v}_{\mathrm{LNA}_c} = -\tilde{\mathbf{Z}}_{\mathrm{eqM_2}}\mathbf{i}_{\mathrm{LNA}}, \tag{2.38}$$

and therefore a transfer function of

$$\mathbf{H}_{\mathrm{L,LNAv,dir}} = R_{\mathrm{L}}\mathbf{I}_{N_R}(R_{\mathrm{L}}\mathbf{I}_{N_R} + \tilde{\mathbf{Z}}_{\mathrm{eqLNA_2}})^{-1}\mathbf{e} \cdot (\mathbf{c} + \tilde{\mathbf{Z}}_{\mathrm{eqM_2}})^{-1}, \tag{2.39}$$

for the series voltages and

$$\begin{aligned} \mathbf{H}_{\mathrm{L,LNAc,dir}} &= -R_{\mathrm{L}}\mathbf{I}_{N_R}(R_{\mathrm{L}}\mathbf{I}_{N_R} + \tilde{\mathbf{Z}}_{\mathrm{eqLNA_2}})^{-1}\mathbf{e} \cdot (\mathbf{c} + \tilde{\mathbf{Z}}_{\mathrm{eqM_2}})^{-1}\tilde{\mathbf{Z}}_{\mathrm{eqM_2}} \\ &= -\mathbf{H}_{\mathrm{L,LNAv,dir}} \cdot \tilde{\mathbf{Z}}_{\mathrm{eqM_2}} \end{aligned} \tag{2.40}$$

for the LNA noise currents. Both transfer functions assume user i to be the receiver. It is clear to see that both transfer functions are of size $\mathbb{C}^{N_{\mathrm{Rx}} \times N_{\mathrm{Rx}}}$.

Indirect LNA Noise Contribution: In a second step, we transfer the LNA-voltage and -current sources to parallel voltage sources at the antennas, so that the transfer function derived in Equation (2.29) can be applied. In the following, all indices are neglected for simplicity reasons. For the transfer functions towards the antennas, we consider all the ports of the passive receivers. Therefore we are looking at matrices of size $\mathbb{C}^{(N_{\mathrm{R}}-1)N_{\mathrm{Rx}} \times (N_{\mathrm{R}}-1)N_{\mathrm{Rx}}}$.

By multiplying the LNA-current noise source by the equivalent input impedance of the LNA

$$\mathbf{v}_{\mathrm{LNAc}} = \mathbf{Z}_{\mathrm{eqLNA1}}\mathbf{i}_{\mathrm{LNA}}, \tag{2.41}$$

the LNA-current noise is transferred to a series voltage, just like the LNA-voltage noise. Now we only need to find the transfer function for the LNA-voltage source $\mathbf{v}_{\mathrm{LNAv}}$. The transfer function over the matching network is given by

$$\mathbf{H}_{\mathrm{O,LNA}} = \mathbf{Z}_{\mathrm{M12}}(\mathbf{Z}_{\mathrm{M22}} + \mathbf{Z}_{\mathrm{eqLNA1}})^{-1}. \tag{2.42}$$

This leads to the overall indirect LNA noise transfer functions of

$$\begin{aligned} \mathbf{H}_{\mathrm{L,LNAv,ind}} &= \mathbf{H}_{\mathrm{L,i}} \cdot \mathbf{H}_{\mathrm{O,LNA}}, \quad \text{for the voltage sources, and} \\ \mathbf{H}_{\mathrm{L,LNAc,ind}} &= \mathbf{H}_{\mathrm{L,LNAv,ind}} \cdot \mathbf{Z}_{\mathrm{eqLNA1}}, \quad \text{for the current sources.} \end{aligned} \tag{2.43}$$

Looking at the size of the matrices we see that the $\mathbf{H}_{\mathrm{O,LNA}}$ as well as $\mathbf{Z}_{\mathrm{eqLNA1}}$ are of size $\mathbb{C}^{(N_{\mathrm{R}}-1)N_{\mathrm{Rx}}\times(N_{\mathrm{R}}-1)N_{\mathrm{Rx}}}$, and therefore the overall transfer function is of size $\mathbb{C}^{N_{\mathrm{Rx}}\times(N_{\mathrm{R}}-1)N_{\mathrm{Rx}}}$.

2.3.3 Downstream Noise

The last noise source is downstream noise, generated by the circuitry after the LNA [11] and modeled by voltage sources $\tilde{\mathbf{v}}_{\mathrm{n}}$ in series to the loads. It has the statistical property

$$\mathbb{E}[\tilde{\mathbf{v}}_{\mathrm{n}}\tilde{\mathbf{v}}_{\mathrm{n}}^{H}] = \psi \cdot \mathbf{I}_{N_{\mathrm{R}}N_{\mathrm{Rx}}}. \tag{2.44}$$

Transfer Function of the Downstream Noise

For the transfer function of the downstream noise we need a simple voltage divider for the loads and the equivalent input impedance $\tilde{\mathbf{Z}}_{\mathrm{eqLNA}_2}$. Looking from the right into the LNA block,

$$\mathbf{H}_{\mathrm{L,n}} = R_{\mathrm{L}}\mathbf{I}_{N_R}(R_{\mathrm{L}}\mathbf{I}_{N_R} + \tilde{\mathbf{Z}}_{\mathrm{eqLNA}_2})^{-1}, \tag{2.45}$$

with

$$\tilde{\mathbf{Z}}_{\mathrm{eqLNA}_2} = \mathbf{g} - \mathbf{d} \cdot (\mathbf{c} + \tilde{\mathbf{Z}}_{\mathrm{eqM}_2})^{-1} \cdot \mathbf{e} = \mathbf{g}, \tag{2.46}$$

where the unilateral assumption ($\mathbf{d} = \mathbf{0}$) was applied, and hence $\tilde{\mathbf{Z}}_{\mathrm{eqLNA}_2} = \mathbf{Z}_{\mathrm{eqLNA}_2}$ from Equation (2.20).

For the downstream noise we note that, under the unilateral assumption, the noise transferred to the antennas is zero because

$$\mathbf{v}_{\mathrm{LNAn}} = \mathbf{d}(\mathbf{g} + R_{\mathrm{L}}\mathbf{I}_{N_R})^{-1}\tilde{\mathbf{v}}_v = \mathbf{0} \tag{2.47}$$

when $\mathbf{d} = 0$. Therefore, the downstream noise only contributes to its own receiver branch, hence $\mathbf{H}_{\mathrm{L,n}}$ is of size $\mathbb{C}^{N_{\mathrm{Rx}}\times N_{\mathrm{Rx}}}$.

2.3.4 Noise Covariance Matrix

In the following, we describe the whole system by its noise transfer functions. We use the index i for the branches of the active receivers and index j for the branches of the passive receiver — the branches that contributed only by their couplings.

With the transfer functions derived for each noise source, we can finally express each noise contribution at the loads as stated in Equation (2.33) by

$$\begin{aligned} \mathbf{u}_{\mathrm{AR}} &= \mathbf{H}_{\mathrm{L},0} \cdot \mathbf{n}_{\mathrm{AR}}, \\ \mathbf{u}_{\mathrm{LNA}_v} &= \mathbf{H}_{\mathrm{L,LNAv,ind}} \cdot \mathbf{v}_{\mathrm{LNA},j} + \mathbf{H}_{\mathrm{L,LNAv,dir}} \cdot \mathbf{v}_{\mathrm{LNA},i}, \\ \mathbf{u}_{\mathrm{LNA}_c} &= \mathbf{H}_{\mathrm{L,LNAc,ind}} \cdot \mathbf{i}_{\mathrm{LNA},j} + \mathbf{H}_{\mathrm{L,LNAc,dir}} \cdot \mathbf{i}_{\mathrm{LNA},i}, \\ \mathbf{u}_{\tilde{n}} &= \mathbf{H}_{\mathrm{L,n}} \cdot \tilde{\mathbf{v}}_n, \\ \text{and therefore} \qquad \mathbf{u}_{\mathrm{L}} &= \mathbf{u}_{\mathrm{AR}} + \mathbf{u}_{\mathrm{LNA}_v} + \mathbf{u}_{\mathrm{LNA}_c} + \mathbf{u}_{\tilde{n}}. \end{aligned} \tag{2.48}$$

As each vector is of size $\mathbb{C}^{N_{\mathrm{Rx}} \times 1}$, the noise covariance matrix described here is of size $\mathbb{C}^{N_{\mathrm{Rx}} \times N_{\mathrm{Rx}}}$. Because all the noise sources are uncorrelated, except for the LNA noise sources (c.f. Equation (2.36)), the noice covariance matrix can be written as:

$$\begin{aligned} \mathbf{K}_{\mathrm{N},i} = \mathbb{E}[\mathbf{u}_{\mathrm{L}} \mathbf{u}_{\mathrm{L}}^H] = \mathbb{E}[\mathbf{u}_{\mathrm{AR}} \mathbf{u}_{\mathrm{AR}}^H] + \mathbb{E}[\mathbf{u}_{\mathrm{LNA}_v} \mathbf{u}_{\mathrm{LNA}_v}^H] + \mathbb{E}[\mathbf{u}_{\mathrm{LNA}_v} \mathbf{u}_{\mathrm{LNA}_c}^H] + \\ \mathbb{E}[\mathbf{u}_{\mathrm{LNA}_c} \mathbf{u}_{\mathrm{LNA}_v}^H] + \mathbb{E}[\mathbf{u}_{\mathrm{LNA}_c} \mathbf{u}_{\mathrm{LNA}_c}^H] + \mathbb{E}[\mathbf{u}_{\tilde{n}} \mathbf{u}_{\tilde{n}}^H]. \end{aligned} \tag{2.49}$$

For simplicity reasons, we will look at each summand separately in the following. For the antenna noise it follows that

$$\mathbb{E}[\mathbf{u}_{\mathrm{AR}} \mathbf{u}_{\mathrm{AR}}^H] = \mathbf{H}_{\mathrm{L,i}} \mathbb{E}[\mathbf{n}_{\mathrm{AR}} \mathbf{n}_{\mathrm{AR}}^H] \mathbf{H}_{\mathrm{L,i}}^H = \mathbf{H}_{\mathrm{L,i}} \mathbf{R}_{\mathrm{na}} \mathbf{H}_{\mathrm{L,i}}^H, \tag{2.50}$$

using (2.34), with $\mathbf{R}_{\mathrm{na}}$ of size $\mathbb{R}^{N_{\mathrm{R}} \cdot (N_{\mathrm{Rx}} + N_{\mathrm{Rel}}) \times N_{\mathrm{R}} \cdot (N_{\mathrm{Rx}} + N_{\mathrm{Rel}})}$. Hence, by the shape of $\mathbf{H}_{\mathrm{L,i}}$, $\mathbb{E}[\mathbf{u}_{\mathrm{AR}} \mathbf{u}_{\mathrm{AR}}^H]$, it becomes a matrix of size $\mathbb{C}^{N_{\mathrm{Rx}} \times N_{\mathrm{Rx}}}$.

For the LNA voltage noise, using (2.36), it follows that

$$\begin{aligned} \mathbb{E}[\mathbf{u}_{\mathrm{LNA}_v} \mathbf{u}_{\mathrm{LNA}_v}^H] = \mathbb{E}[(\mathbf{H}_{\mathrm{L,LNAv,ind}} \cdot \mathbf{v}_{\mathrm{LNA},j} + \mathbf{H}_{\mathrm{L,LNAv,dir}} \cdot \mathbf{v}_{\mathrm{LNA},i}) \cdot \\ (\mathbf{H}_{\mathrm{L,LNAv,ind}} \cdot \mathbf{v}_{\mathrm{LNA},j} + \mathbf{H}_{\mathrm{L,LNAv,dir}} \cdot \mathbf{v}_{\mathrm{LNA},i})^H]. \end{aligned} \tag{2.51}$$

Because $\mathbf{v}_{\mathrm{LNA},j}$ and $\mathbf{v}_{\mathrm{LNA},i}$ are independent of each other (c.f. Equation (2.36)), the cross terms cancel out and

$$\begin{aligned} \mathbb{E}[\mathbf{u}_{\mathrm{LNA}_v} \mathbf{u}_{\mathrm{LNA}_v}^H] &= \mathbf{H}_{\mathrm{L,LNAv,ind}} \cdot \mathbb{E}[\mathbf{v}_{\mathrm{LNA},j} \mathbf{v}_{\mathrm{LNA},j}^H] \cdot \mathbf{H}_{\mathrm{L,LNAv,ind}}^H + \\ &\quad \mathbf{H}_{\mathrm{L,LNAv,dir}} \cdot \mathbb{E}[\mathbf{v}_{\mathrm{LNA},i} \mathbf{v}_{\mathrm{LNA},i}^H] \cdot \mathbf{H}_{\mathrm{L,LNAv,dir}}^H \\ &= \left(\mathbf{H}_{\mathrm{L,LNAv,ind}} \cdot \mathbf{H}_{\mathrm{L,LNAv,ind}}^H + \mathbf{H}_{\mathrm{L,LNAv,dir}} \cdot \mathbf{H}_{\mathrm{L,LNAv,dir}}^H\right) \cdot \beta \cdot R_n^2 \end{aligned} \tag{2.52}$$

for the LNA-voltage source. Similar for the current source,

$$\mathbb{E}[\mathbf{u}_{\mathrm{LNA}_c} \mathbf{u}_{\mathrm{LNA}_c}^H] = \left(\mathbf{H}_{\mathrm{L,LNAc,ind}} \cdot \mathbf{H}_{\mathrm{L,LNAc,ind}}^H + \mathbf{H}_{\mathrm{L,LNAc,dir}} \cdot \mathbf{H}_{\mathrm{L,LNAc,dir}}^H\right) \cdot \beta. \tag{2.53}$$

The remaining terms for the LNA noise contribution are the cross terms. For

them it follows that

$$\begin{aligned}\mathbb{E}[\mathbf{u}_{\mathrm{LNA}_c}\mathbf{u}_{\mathrm{LNA}_v}^H]+\mathbb{E}[\mathbf{u}_{\mathrm{LNA}_c}\mathbf{u}_{\mathrm{LNA}_c}^H] &= \mathbf{H}_{\mathrm{L,LNAv,dir}}\cdot\rho\beta\cdot R_n\cdot\mathbf{H}_{\mathrm{L,LNAc,dir}}^H+\\ &\mathbf{H}_{\mathrm{L,LNAc,dir}}\cdot\rho^*\beta\cdot R_n\cdot\mathbf{H}_{\mathrm{L,LNAv,dir}}^H+\\ &\mathbf{H}_{\mathrm{L,0}}\cdot\mathbf{H}_{\mathrm{L,LNAv,ind}}\cdot\rho\beta\cdot R_n\cdot\mathbf{H}_{\mathrm{L,LNAc,ind}}^H\mathbf{H}_{\mathrm{L,0}}^H+\\ &\mathbf{H}_{\mathrm{L,0}}\cdot\mathbf{H}_{\mathrm{L,LNAc,ind}}\cdot\rho^*\beta\cdot R_n\cdot\mathbf{H}_{\mathrm{L,LNAv,ind}}^H\mathbf{H}_{\mathrm{L,0}}^H\\ &= \beta\cdot R_n\Big(-\mathbf{H}_{\mathrm{L,LNAv,dir}}\left(\rho\tilde{\mathbf{Z}}_{\mathrm{eqM_2}}^H+\tilde{\mathbf{Z}}_{\mathrm{eqM_2}}\rho^*\right)\mathbf{H}_{\mathrm{L,LNAv,dir}}+\\ &\mathbf{H}_{\mathrm{L,LNAv,ind}}\left(\rho\mathbf{Z}_{\mathrm{eqLNA_1}}^H+\mathbf{Z}_{\mathrm{eqLNA_1}}\rho^*\right)\mathbf{H}_{\mathrm{L,LNAv,ind}}\Big)\\ &= 2\beta\cdot R_n\Big(-\mathbf{H}_{\mathrm{L,LNAv,dir}}\cdot\mathbb{R}\{\rho^*\tilde{\mathbf{Z}}_{\mathrm{eqM_2}}\}\cdot\mathbf{H}_{\mathrm{L,LNAv,dir}}+\\ &\mathbf{H}_{\mathrm{L,LNAv,ind}}\cdot\mathbb{R}\{\rho^*\mathbf{Z}_{\mathrm{eqLNA_1}}\}\cdot\mathbf{H}_{\mathrm{L,LNAv,ind}}\Big),\end{aligned}\tag{2.54}$$

where Equations (2.36), (2.40) and (2.43) are used.

Finally, there is only the downstream noise contribution remaining. Because of the unilateral assumption, this becomes less complex, and

$$\mathbb{E}[\mathbf{u}_{\tilde{n}}\mathbf{u}_{\tilde{n}}^H]=\psi\cdot\mathbf{H}_{\mathrm{L,n}}\cdot\mathbf{H}_{\mathrm{L,n}}^H,$$

where the statistical property of the downstream noise from Equation (2.44) is used.

With these results we can form the final noise covariance matrix as

$$\begin{aligned}\mathbf{K}_{\mathrm{N},i} &= \mathbf{H}_{\mathrm{L,i}}\mathbf{R}_{\mathrm{na}}\mathbf{H}_{\mathrm{L,i}}^H+\\ &\beta\cdot R_n^2\cdot\left(\mathbf{H}_{\mathrm{L,LNAv,ind}}\cdot\mathbf{H}_{\mathrm{L,LNAv,ind}}^H+\mathbf{H}_{\mathrm{L,LNAv,dir}}\cdot\mathbf{H}_{\mathrm{L,LNAv,dir}}^H\right)+\\ &\beta\cdot\left(\mathbf{H}_{\mathrm{L,LNAc,ind}}\cdot\mathbf{H}_{\mathrm{L,LNAc,ind}}^H+\mathbf{H}_{\mathrm{L,LNAc,dir}}\cdot\mathbf{H}_{\mathrm{L,LNAc,dir}}^H\right)+\\ &2\beta\cdot R_n\Big(-\mathbf{H}_{\mathrm{L,LNAv,dir}}\cdot\mathbb{R}\{\rho^*\tilde{\mathbf{Z}}_{\mathrm{eqM_2}}\}\cdot\mathbf{H}_{\mathrm{L,LNAv,dir}}+\\ &\mathbf{H}_{\mathrm{L,LNAv,ind}}\cdot\mathbb{R}\{\rho^*\mathbf{Z}_{\mathrm{eqLNA_1}}\}\cdot\mathbf{H}_{\mathrm{L,LNAv,ind}}\Big)+\\ &\psi\cdot\mathbf{H}_{\mathrm{L,n}}\cdot\mathbf{H}_{\mathrm{L,n}}^H.\end{aligned}\tag{2.55}$$

According to the noise vector sizes given in the beginning of this section, the noise covariance matrix is of size $\mathbb{C}^{N_{\mathrm{Rx}}\times N_{\mathrm{Rx}}}$.

2.4 Rate Calculations

2.4.1 Achievable Rate

After the derivation of the signal, interference, and noise covariance matrices, we can now describe the achievable rate for each connection pair. The achievable rate for user j is described as

$$\begin{aligned}r_j &= \log_2\left(\det\left(\mathbf{K}_{\mathrm{S},j}\left(\mathbf{K}_{\mathrm{I},j}+\mathbf{K}_{\mathrm{N},j}\right)^{-1}+\mathbf{I}_{N_R}\right)\right)\\ &= \log_2\left(\det\left(\mathbf{K}_{\mathrm{S},j}+\mathbf{K}_{\mathrm{I},j}+\mathbf{K}_{\mathrm{N},j}\right)\right)-\log_2\left(\det\left(\mathbf{K}_{\mathrm{I},j}+\mathbf{K}_{\mathrm{N},j}\right)\right).\end{aligned}\tag{2.56}$$

Stacking the achievable rates for each user into a vector leads to

$$\mathbf{r}=\begin{bmatrix}r_0 & r_1 & \cdots & r_{N_{\mathrm{User}}-1}\end{bmatrix}^T.\tag{2.57}$$

By this vector, we can describe the achievable sum rate as

$$r_{\mathrm{Sum}} = ||\mathbf{r}||_1, \tag{2.58}$$

where $||\cdot||_1$ is the 1-norm, or the sum of the elements of $\mathbf{r}$:

$$\max_{\mathbf{Z}_{\mathrm{M}},\mathbf{X}_{\mathrm{Rel}}} (r_{\mathrm{Sum}}) = \max_{\mathbf{Z}_{\mathrm{M}},\mathbf{X}_{\mathrm{Rel}}} \left(\sum_{j=0}^{N_{\mathrm{User}}-1} r[j] \right). \tag{2.59}$$

2.4.2 Interference Limited or Noise Free Rate

Another measure required in this thesis is the interference limited or noise-free rate. It is calculated by only considering signal and interference power at the loads. Therefore, neglecting the noise in Equation 2.56 leads to

$$r_j = \log_2 \left(\det \left(\mathbf{K}_{\mathrm{S},j} + \mathbf{K}_{\mathrm{I},j} \right) \right) - \log_2 \left(\det \left(\mathbf{K}_{\mathrm{I},j} \right) \right). \tag{2.60}$$

This is helpful for seeing how well the interference is removed by our optimization, which will be introduced in Chapter 4. The noise-free rate also will be denoted as the SIR-rate.

2.4.3 TDMA Rate

In later sections, the results achieved in this thesis are compared to existing protocols for eliminating interference, such as TDMA. Therefore, in the following the achievable rates for the TDMA protocol will be shown.

Time in TDMA is split up in slots in which each user is allowed to transmit without any interference, so the achievable rate from Equation (2.56) reduces to the interference-free achievable rate of

$$r_j = \frac{1}{N_{\mathrm{User}}} \cdot \left(\log_2 \left(\det \left(\mathbf{K}_{\mathrm{S},j} + \mathbf{K}_{\mathrm{N},j} \right) \right) - \log_2 \left(\det \left(\mathbf{K}_{\mathrm{N},j} \right) \right) \right). \tag{2.61}$$

It is obvious that, with no interference, this rate would be higher than the achievable rate with interference if the factor of $\frac{1}{N_{\mathrm{User}}}$ was not considered. However users are no longer allowed, to use the full transmission period, but rather only a time slot of length $\frac{1}{N_{\mathrm{User}}} \cdot T_0$, where T_0 denotes the length of the full transmission period. Therefore, the achievable sum rate can be written as

$$\begin{aligned} r_{\mathrm{Sum}} &= ||\mathbf{r}||_1, \\ &= \frac{1}{N_{\mathrm{User}}} \cdot \sum_{j=0}^{N_{\mathrm{User}}-1} r_j. \end{aligned} \tag{2.62}$$

The term $\frac{1}{N_{\mathrm{User}}}$ is hereafter called "pre-log" factor, and is the reason TDMA is not a good approach for a large number of users, as N_{User} increases linearly while the advantage of an interference-free link only increases logarithmically.

There are different approaches to use TDMA, such as allowing a small number of users at the same time to transmit during one time slot. This will lead to some interference but therefore also to a smaller pre-log factor. Such an approach is used in the later chapters.

Chapter 3

Analytical Gradient

In the following, the derivation of the gradients is given. In the first section, the signal gradients are derived, in the later section we derive the noise gradients. The gradients are used to improve the achievable rates of the system (Equation (2.56)). We are interested in the gradient of the achievable rates with respect to the matching network and the passive antenna loads. Using the matrix relations from [12] and restricting to the achievable sum rate, the gradient becomes

$$\frac{\partial \mathbf{r}}{\partial \mathbf{Z}_{l,ij}} = \sum_{i=0}^{N_{\text{User}}-1} \frac{\partial r_i}{\partial \mathbf{Z}_{l,ij}}. \tag{3.1}$$

Therefore, the gradient must be derived for each user, and looking at one and applying it to the others is sufficient. The gradient of one user (neglecting the user index for simplicity reasons) can be written as

$$\frac{\partial r}{\partial \mathbf{Z}_{l,ij}} = \frac{1}{\ln(2)} \text{Tr}\Bigg((\mathbf{K}_\text{s} + \mathbf{K}_\text{i} + \mathbf{K}_\text{n})^{-1} \left(\frac{\partial \mathbf{K}_\text{s}}{\partial \mathbf{Z}_{l,ij}} + \frac{\partial \mathbf{K}_\text{i}}{\partial \mathbf{Z}_{l,ij}} + \frac{\partial \mathbf{K}_\text{n}}{\partial \mathbf{Z}_{l,ij}} \right) - \tag{3.2}$$

$$(\mathbf{K}_\text{s} + \mathbf{K}_\text{n})^{-1} \left(\frac{\partial \mathbf{K}_\text{i}}{\partial \mathbf{Z}_{l,ij}} + \frac{\partial \mathbf{K}_\text{n}}{\partial \mathbf{Z}_{l,ij}} \right) \Bigg), \tag{3.3}$$

with $l \in \{\text{M11}, \text{M12}, \text{M22}, \text{pass}\}$ denoting the sub-matrices of the matching network or the passive antenna loads and i, j denoting the element in the i-th row and j-th column. In the following, the gradient is split up in to the signal, interference, and noise part. The derivatives for each covariance matrix are determined.

3.1 Signal Gradient

For the signal covariance matrix, we see from Equation (2.31) that we can take the derivative of each sub-transfer function and place them together after by the chain rule. Therefore, the gradient of the signal covariance becomes

$$\frac{\partial \mathbf{K}_s}{\partial \mathbf{Z}_{l,ij}} = \frac{\partial \mathbf{H}_{\text{L},0}}{\partial \mathbf{Z}_{l,ij}} \cdot \mathbf{H}_0^{\text{sp}} \cdot \mathbb{E}[\mathbf{v}_0 \mathbf{v}_0^H] \cdot {\mathbf{H}_0^{\text{sp}}}^H \cdot \mathbf{H}_{\text{L},0}^H +$$

$$\mathbf{H}_{\text{L},0} \cdot \mathbf{H}_0^{\text{sp}} \cdot \mathbb{E}[\mathbf{v}_0 \mathbf{v}_0^H] \cdot {\mathbf{H}_0^{\text{sp}}}^H \cdot \frac{\partial \mathbf{H}_{\text{L},0}^H}{\partial \mathbf{Z}_{l,ij}}. \tag{3.4}$$

First we check which sub-transfer functions (c.f. Equation (2.30)) are affected by the gradient. We see that the transfer functions $\mathbf{H}_{\text{LNA,M}}$, $\mathbf{H}_{\text{M},0'}$, and obviously $\mathbf{H}_i^{\text{pr}}$ for port reduction are affected by the relay loads and the matching network.

For the following, $\mathbf{J}_{ij}$ denotes the single entry matrix, with respect to the i-th row and the j-th column. It follows for the port reduction transfer function (again neglecting the user index) that

$$\frac{\partial \mathbf{H}^{\mathrm{pr}}}{\partial \mathbf{Z}_{\mathrm{pass},ij}} = \begin{bmatrix} \mathbf{0}_{N_{\mathrm{Rx}}} & \mathbf{Z}_{\mathrm{OL}}(\mathbf{Z}_{\mathrm{pass}} + \mathbf{Z}_{\mathrm{LL}})^{-1}\mathbf{J}_{ij}(\mathbf{Z}_{\mathrm{pass}} + \mathbf{Z}_{\mathrm{LL}})^{-1} \end{bmatrix} \tag{3.5}$$

with $\mathbf{0}_{N_{\mathrm{Rx}}}$ — the N_{Rx} by N_{Rx} all-zeros matrix.

Next, for the voltage divider before the matching network — the transfer function of the open circuit voltages at the antennas to parallel input voltages of the matching network — it follows that

$$\frac{\partial \mathbf{H}_{\mathrm{M,0'}}}{\partial \mathbf{Z}_{11,ij}} = \mathbf{J}_{ij}(\mathbf{Z}_{\mathrm{eqM_1}} + \mathbf{Z}_{\mathrm{C'}})^{-1} - \mathbf{Z}_{\mathrm{eqM_1}}(\mathbf{Z}_{\mathrm{eqM_1}} + \mathbf{Z}_{\mathrm{C'}})^{-1}\mathbf{J}_{ij}(\mathbf{Z}_{\mathrm{eqM_1}} + \mathbf{Z}_{\mathrm{C'}})^{-1}, \tag{3.6}$$

$$\text{with} \quad \frac{\partial \mathbf{Z}_{\mathrm{eqM_1}}}{\partial \mathbf{Z}_{\mathrm{M12}}} = \mathbf{J}_{ij}^{T}(\mathbf{Z}_{\mathrm{M22}} + \mathbf{Z}_{\mathrm{eqLNA_1}})^{-1}\mathbf{Z}_{\mathrm{M12}} + \mathbf{Z}_{\mathrm{M12}}^{T}(\mathbf{Z}_{\mathrm{M22}} + \mathbf{Z}_{\mathrm{eqLNA_1}})^{-1}\mathbf{J}_{ij},$$

$$\begin{aligned} \frac{\partial \mathbf{H}_{\mathrm{M,0'}}}{\partial \mathbf{Z}_{12,ij}} = {} & \frac{\partial \mathbf{Z}_{\mathrm{eqM_1}}}{\partial \mathbf{Z}_{\mathrm{M12}}}(\mathbf{Z}_{\mathrm{eqM_1}} + \mathbf{Z}_{\mathrm{C'}})^{-1} - \\ & \mathbf{Z}_{\mathrm{eqM_1}}(\mathbf{Z}_{\mathrm{eqM_1}} + \mathbf{Z}_{\mathrm{C'}})^{-1}\frac{\partial \mathbf{Z}_{\mathrm{eqM_1}}}{\partial \mathbf{Z}_{\mathrm{M12}}}(\mathbf{Z}_{\mathrm{eqM_1}} + \mathbf{Z}_{\mathrm{C'}})^{-1}, \end{aligned} \tag{3.7}$$

$$\text{with} \quad \frac{\partial \mathbf{Z}_{\mathrm{eqM_1}}}{\partial \mathbf{Z}_{\mathrm{M22}}} = \mathbf{Z}_{\mathrm{M12}}^{T}(\mathbf{Z}_{\mathrm{M22}} + \mathbf{Z}_{\mathrm{eqLNA_1}})^{-1}\mathbf{J}_{ij}^{T}(\mathbf{Z}_{\mathrm{M22}} + \mathbf{Z}_{\mathrm{eqLNA_1}})^{-1}\mathbf{Z}_{\mathrm{M12}},$$

$$\begin{aligned} \frac{\partial \mathbf{H}_{\mathrm{M,0'}}}{\partial \mathbf{Z}_{22,ij}} = {} & \frac{\partial \mathbf{Z}_{\mathrm{eqM_1}}}{\partial \mathbf{Z}_{\mathrm{M22}}}(\mathbf{Z}_{\mathrm{eqM_1}} + \mathbf{Z}_{\mathrm{C'}})^{-1} - \\ & \mathbf{Z}_{\mathrm{eqM_1}}(\mathbf{Z}_{\mathrm{eqM_1}} + \mathbf{Z}_{\mathrm{C'}})^{-1}\frac{\partial \mathbf{Z}_{\mathrm{eqM_1}}}{\partial \mathbf{Z}_{\mathrm{M22}}}(\mathbf{Z}_{\mathrm{eqM_1}} + \mathbf{Z}_{\mathrm{C'}})^{-1}, \end{aligned} \tag{3.8}$$

$$\text{and with} \quad \frac{\partial \mathbf{Z}_{\mathrm{C'}}}{\partial \mathbf{Z}_{\mathrm{pass},ij}} = \mathbf{Z}_{\mathrm{OL}}(\mathbf{Z}_{\mathrm{pass}} + \mathbf{Z}_{\mathrm{LL}})^{-1}\mathbf{J}_{ij}(\mathbf{Z}_{\mathrm{pass}} + \mathbf{Z}_{\mathrm{LL}})^{-1}\mathbf{Z}_{\mathrm{LO}}$$

$$\frac{\partial \mathbf{H}_{\mathrm{M,0'}}}{\partial \mathbf{Z}_{\mathrm{pass},ij}} = -\mathbf{Z}_{\mathrm{eqM_1}}(\mathbf{Z}_{\mathrm{eqM_1}} + \mathbf{Z}_{\mathrm{C'}})^{-1}\frac{\partial \mathbf{Z}_{\mathrm{C'}}}{\partial \mathbf{Z}_{\mathrm{pass},ij}}(\mathbf{Z}_{\mathrm{eqM_1}} + \mathbf{Z}_{\mathrm{C'}})^{-1}. \tag{3.9}$$

After deriving the gradient for the voltage divider transfer function, the transfer function over the matching network is the last remaining affected transfer function. Its gradient can be written as

$$\begin{aligned} \frac{\partial \mathbf{H}_{\mathrm{LNA,M}}}{\partial \mathbf{Z}_{11,ij}} = {} & -\mathbf{H}_{\mathrm{LNA,M}}\mathbf{J}_{ij}\mathbf{Z}_{\mathrm{M11}}^{-1}\mathbf{Z}_{\mathrm{M12}}(\mathbf{Z}_{\mathrm{eqLNA_1}} + \mathbf{Z}_{\mathrm{eqM_2}})^{-1}\mathbf{Z}_{\mathrm{M12}}\mathbf{Z}_{\mathrm{M11}}^{-1} - \\ & \mathbf{H}_{\mathrm{LNA,M}}\mathbf{J}_{ij}\mathbf{Z}_{\mathrm{M11}}^{-1}, \end{aligned} \tag{3.10}$$

$$\begin{aligned} \frac{\partial \mathbf{H}_{\mathrm{LNA,M}}}{\partial \mathbf{Z}_{12,ij}} = {} & -\mathbf{Z}_{\mathrm{eqLNA_1}}(\mathbf{Z}_{\mathrm{eqLNA_1}} + \mathbf{Z}_{\mathrm{eqM_2}})^{-1}\mathbf{J}_{ij}^{T}\mathbf{Z}_{\mathrm{M11}}^{-1}\mathbf{Z}_{\mathrm{M12}} - \\ & \mathbf{Z}_{\mathrm{M12}}^{T}\mathbf{Z}_{\mathrm{M11}}^{-1}\mathbf{J}_{ij}(\mathbf{Z}_{\mathrm{eqLNA_1}} + \mathbf{Z}_{\mathrm{eqM_2}})^{-1}\mathbf{Z}_{\mathrm{M12}}\mathbf{Z}_{\mathrm{M11}}^{-1} + \\ & \mathbf{Z}_{\mathrm{eqLNA_1}}(\mathbf{Z}_{\mathrm{eqLNA_1}} + \mathbf{Z}_{\mathrm{eqM_2}})^{-1}\mathbf{J}_{ij}\mathbf{Z}_{\mathrm{M11}}^{-1}, \quad \text{and} \end{aligned} \tag{3.11}$$

$$\frac{\partial \mathbf{H}_{\mathrm{LNA,M}}}{\partial \mathbf{Z}_{22,ij}} = \mathbf{Z}_{\mathrm{eqLNA_1}}(\mathbf{Z}_{\mathrm{eqLNA_1}} + \mathbf{Z}_{\mathrm{eqM_2}})^{-1}\mathbf{J}_{ij}(\mathbf{Z}_{\mathrm{eqLNA_1}} + \mathbf{Z}_{\mathrm{eqM_2}})^{-1}\mathbf{Z}_{\mathrm{M12}}\mathbf{Z}_{\mathrm{M11}}^{-1}. \tag{3.12}$$

Note that the transfer function is only affected by the matching network and not by the coupling network, hence also not by the relay loads.

3.2 Interference Gradient

From Equation (2.32) it can be seen that the interference is similar to the signal, so the same derivatives as in Section 3.1 will apply to the interference. This leads to the gradient of the interference covariance matrix for user i

$$\frac{\partial \mathbf{K}_{\mathrm{i},i}}{\partial \mathbf{Z}_{l,ij}} = \frac{\partial \mathbf{H}_{\mathrm{L},i}}{\partial \mathbf{Z}_{l,ij}} \cdot \left(\sum_{j=0, j\neq i}^{N_{\mathrm{User}}-1} \mathbf{H}_j^{\mathrm{sp}} \cdot \mathbb{E}[\mathbf{v}_j \mathbf{v}_j^H] \cdot \mathbf{H}_j^{\mathrm{sp}^H} \right) \cdot \mathbf{H}_{\mathrm{L},i}^H + \mathbf{H}_{\mathrm{L},i} \cdot \left(\sum_{j=1}^{N_{\mathrm{User}}-1} \mathbf{H}_j^{\mathrm{sp}} \cdot \mathbb{E}[\mathbf{v}_j \mathbf{v}_j^H] \cdot \mathbf{H}_j^{\mathrm{sp}^H} \right) \cdot \frac{\partial \mathbf{H}_{\mathrm{L},i}^H}{\partial \mathbf{Z}_{l,ij}}. \tag{3.13}$$

Again, only the transfer function $\mathbf{H}_{\mathrm{L,i}}$ is affected by the matching network and the relay loads. Its gradient was shown in Section 3.1, so it is neglected here.

3.3 Noise Gradients

As written in Section 2.3, we have four noise sources, of which only the two LNA noise sources are correlated. From the noise covariance matrix derived in Equation (2.55), the gradient can be written as

$$\begin{aligned}
\frac{\partial \mathbf{K}_{\mathrm{n}}}{\partial \mathbf{Z}_{l,ij}} = {} & \frac{\partial \mathbf{H}_{\mathrm{L},i}}{\partial \mathbf{Z}_{l,ij}} \mathbf{R}_{\mathrm{na}} \mathbf{H}_{\mathrm{L,i}}^H + \mathbf{H}_{\mathrm{L},0} \mathbf{R}_{\mathrm{na}} \frac{\partial \mathbf{H}_{\mathrm{L},i}}{\partial \mathbf{Z}_{l,ij}}^H + \\
& \beta \cdot R_n^2 \cdot \left(\frac{\partial \mathbf{H}_{\mathrm{L,LNAv,ind}}}{\mathbf{Z}_{l,ij}} \cdot \mathbf{H}_{\mathrm{L,LNAv,ind}}^H + \frac{\partial \mathbf{H}_{\mathrm{L,LNAv,dir}}}{\mathbf{Z}_{l,ij}} \cdot \mathbf{H}_{\mathrm{L,LNAv,dir}}^H + \right. \\
& \left. \mathbf{H}_{\mathrm{L,LNAv,ind}} \cdot \frac{\partial \mathbf{H}_{\mathrm{L,LNAv,ind}}^H}{\mathbf{Z}_{l,ij}} + \mathbf{H}_{\mathrm{L,LNAv,dir}} \cdot \frac{\partial \mathbf{H}_{\mathrm{L,LNAv,dir}}^H}{\mathbf{Z}_{l,ij}} \right) + \\
& \beta \cdot \left(\frac{\partial \mathbf{H}_{\mathrm{L,LNAc,ind}}}{\mathbf{Z}_{l,ij}} \cdot \mathbf{H}_{\mathrm{L,LNAc,ind}}^H + \frac{\partial \mathbf{H}_{\mathrm{L,LNAc,dir}}}{\mathbf{Z}_{l,ij}} \cdot \mathbf{H}_{\mathrm{L,LNAc,dir}}^H + \right. \\
& \left. \mathbf{H}_{\mathrm{L,LNAc,ind}} \cdot \frac{\partial \mathbf{H}_{\mathrm{L,LNAc,ind}}^H}{\mathbf{Z}_{l,ij}} + \mathbf{H}_{\mathrm{L,LNAc,dir}} \cdot \frac{\partial \mathbf{H}_{\mathrm{L,LNAc,dir}}^H}{\mathbf{Z}_{l,ij}} \right) + \\
& 2\beta \cdot R_n \left(- \frac{\partial \mathbf{H}_{\mathrm{L,LNAv,dir}}}{\mathbf{Z}_{l,ij}} \cdot \Re\{\rho^* \tilde{\mathbf{Z}}_{\mathrm{eqM}_2}\} \cdot \mathbf{H}_{\mathrm{L,LNAv,dir}} + \right. \\
& \frac{\partial \mathbf{H}_{\mathrm{L,LNAv,ind}}}{\mathbf{Z}_{l,ij}} \cdot \Re\{\rho^* \mathbf{Z}_{\mathrm{eqLNA}_1}\} \cdot \mathbf{H}_{\mathrm{L,LNAv,ind}} \\
& - \mathbf{H}_{\mathrm{L,LNAv,dir}} \cdot \Re\{\rho^* \tilde{\mathbf{Z}}_{\mathrm{eqM}_2}\} \cdot \frac{\partial \mathbf{H}_{\mathrm{L,LNAv,dir}}}{\mathbf{Z}_{l,ij}} + \\
& \left. \mathbf{H}_{\mathrm{L,LNAv,ind}} \cdot \Re\{\rho^* \mathbf{Z}_{\mathrm{eqLNA}_1}\} \cdot \frac{\partial \mathbf{H}_{\mathrm{L,LNAv,ind}}}{\mathbf{Z}_{l,ij}} \right) + \\
& \psi \left(\frac{\partial \mathbf{H}_{\mathrm{L,n}}}{\mathbf{Z}_{l,ij}} \cdot \mathbf{H}_{\mathrm{L,n}}^H + \mathbf{H}_{\mathrm{L,n}} \cdot \frac{\partial \mathbf{H}_{\mathrm{L,n}}^H}{\mathbf{Z}_{l,ij}} \right).
\end{aligned} \tag{3.14}$$

The gradient for the antenna noise ($\frac{\partial \mathbf{H}_{\mathrm{L},i}}{\partial \mathbf{Z}_{l,ij}}$) is the same as the one for the signal. For the LNA noise, we need some new gradients. For the downstream noise contribution it can be shown that — under the unilateral assumption — the transfer function is independent of the matching network and the relay loads, hence the gradient is zero. In the following, the gradients of the sub-covariance matrices are derived and described in more detail.

3.3.1 Antenna Noise Gradient

As the antenna noise is picked up in the same place as the signal, its gradient is also the same as the signal covariance gradient. The formulas from (3.5) to (3.12) apply in the same manner to the antenna noise transfer functions, so they are omitted here. We only note that the transfer functions $\mathbf{H}_0^{\mathrm{pr}}$, $\mathbf{H}_{\mathrm{M},0}$ and $\mathbf{H}_{\mathrm{LNA,M}}$ are affected in the derivation of $\frac{\partial \mathbf{K}_{\mathrm{n}}}{\partial \mathbf{Z}_{l,ij}}$, with $l \in \{\mathrm{M11}, \mathrm{M12}, \mathrm{M22}, \mathrm{pass}\}$.

3.3.2 LNA Noise Gradient

Looking at the transfer function of the two LNA noise sources, we see that the newly introduced $\tilde{\mathbf{Z}}_{\mathrm{eqM}_2}$ (Equation (2.37)) is dependent on the matching network and on the coupling matrix, hence on the relay loads. Further, as the direct transfer function from Equations (2.39) and (2.40) are dependent on $\tilde{\mathbf{Z}}_{\mathrm{eqM}_2}$, their gradient must be derived. Last, the gradient of the indirect transfer functions (Equation (2.43)) must be also derived.

Gradient of the Direct Noise Contribution

First, we show the gradient of the newly introduced equivalent impedance matrix $\tilde{\mathbf{Z}}_{\mathrm{eqM}_2}$. It can be written as

$$\frac{\partial \tilde{\mathbf{Z}}_{\mathrm{eqM}_2}}{\partial \mathbf{Z}_{11,ij}} = \mathbf{Z}_{\mathrm{M12}}(\mathbf{Z}_{\mathrm{M11}} + \mathbf{Z}_{\mathrm{C'}})^{-1}\mathbf{J}_{ij}(\mathbf{Z}_{\mathrm{M11}} + \mathbf{Z}_{\mathrm{C'}})^{-1}, \tag{3.15}$$

$$\frac{\partial \tilde{\mathbf{Z}}_{\mathrm{eqM}_2}}{\partial \mathbf{Z}_{12,ij}} = -\mathbf{J}_{ij}(\mathbf{Z}_{\mathrm{M11}} + \mathbf{Z}_{\mathrm{C'}})^{-1}\mathbf{Z}_{\mathrm{M21}} - \mathbf{Z}_{\mathrm{M12}}(\mathbf{Z}_{\mathrm{M11}} + \mathbf{Z}_{\mathrm{C'}})^{-1}\mathbf{J}_{ij}^T, \tag{3.16}$$

$$\frac{\partial \tilde{\mathbf{Z}}_{\mathrm{eqM}_2}}{\partial \mathbf{Z}_{22,ij}} = \mathbf{J}_{ij}, \tag{3.17}$$

$$\text{and with} \quad \frac{\partial \mathbf{Z}_{\mathrm{C'}}}{\partial \mathbf{Z}_{\mathrm{pass},ij}} = \mathbf{Z}_{\mathrm{OL}}(\mathbf{Z}_{\mathrm{pass}} + \mathbf{Z}_{\mathrm{LL}})^{-1}\mathbf{J}_{ij}(\mathbf{Z}_{\mathrm{pass}} + \mathbf{Z}_{\mathrm{LL}})^{-1}\mathbf{Z}_{\mathrm{LO}},$$

$$\frac{\partial \tilde{\mathbf{Z}}_{\mathrm{eqM}_2}}{\partial \mathbf{Z}_{\mathrm{pass},ij}} = \mathbf{Z}_{\mathrm{M12}}(\mathbf{Z}_{\mathrm{M11}} + \mathbf{Z}_{\mathrm{C'}})^{-1}\frac{\partial \mathbf{Z}_{\mathrm{C'}}}{\partial \mathbf{Z}_{\mathrm{pass},ij}}(\mathbf{Z}_{\mathrm{M11}} + \mathbf{Z}_{\mathrm{C'}})^{-1}\mathbf{Z}_{\mathrm{M21}}. \tag{3.18}$$

Therefore, the direct transfer functions from Equation (2.39) and (2.40) can be expressed by

$$\frac{\partial \mathbf{H}_{\mathrm{L,LNAv,dir}}}{\partial \mathbf{Z}_{l,ij}} = -R_{\mathrm{L}}\mathbf{I}_{N_R}(R_{\mathrm{L}}\mathbf{I}_{N_R} + \tilde{\mathbf{Z}}_{\mathrm{eqLNA}_2})^{-1}\mathbf{e}\cdot(\mathbf{c} + \tilde{\mathbf{Z}}_{\mathrm{eqM}_2})^{-1}\cdot \frac{\partial \tilde{\mathbf{Z}}_{\mathrm{eqM}_2}}{\partial \mathbf{Z}_{l,ij}}\cdot(\mathbf{c} + \tilde{\mathbf{Z}}_{\mathrm{eqM}_2})^{-1}, \quad \text{and} \tag{3.19}$$

$$\frac{\partial \mathbf{H}_{\mathrm{L,LNAc,dir}}}{\partial \mathbf{Z}_{l,ij}} = -\frac{\partial \mathbf{H}_{\mathrm{L,LNAv,dir}}}{\partial \mathbf{Z}_{l,ij}}\cdot\tilde{\mathbf{Z}}_{\mathrm{eqM}_2} - \mathbf{H}_{\mathrm{L,LNAv,dir}}\cdot\frac{\partial \tilde{\mathbf{Z}}_{\mathrm{eqM}_2}}{\partial \mathbf{Z}_{l,ij}}. \tag{3.20}$$

Gradient of the Indirect Noise Contribution

The indirect transfer function consists of two parts: the sub-function $\mathbf{H}_{\mathrm{O,LNA}}$ to transfer the signal towards the antennas, and the sub-function $\mathbf{H}_{\mathrm{L},i}$ to transfer the noise towards the loads over the coupling. The gradient of the second function was already derived for the signal, so it is neglected here. Therefore the gradient of

$\mathbf{H}_{\mathrm{O,LNA}}$ is given by

$$\frac{\partial \mathbf{H}_{\mathrm{O,LNA}}}{\partial \mathbf{Z}_{M12,ij}} = \mathbf{J}_{ij}(\mathbf{Z}_{\mathrm{M22}} + \mathbf{Z}_{\mathrm{eqLNA1}})^{-1}, \quad \text{and} \tag{3.21}$$

$$\frac{\partial \mathbf{H}_{\mathrm{O,LNA}}}{\partial \mathbf{Z}_{M22,ij}} = -\mathbf{Z}_{\mathrm{M12}}(\mathbf{Z}_{\mathrm{M22}} + \mathbf{Z}_{\mathrm{eqLNA1}})^{-1} \cdot \mathbf{J}_{ij}(\mathbf{Z}_{\mathrm{M22}} + \mathbf{Z}_{\mathrm{eqLNA1}})^{-1}, \tag{3.22}$$

as $\mathbf{H}_{\mathrm{O,LNA}}$ is independent of $\mathbf{Z}_{11}$ and $\mathbf{Z}_{\mathrm{Pass}}$, it is zero in those cases. This leads to the gradient of the indirect transfer function, given by

$$\frac{\partial \mathbf{H}_{\mathrm{L,LNAv,ind}}}{\partial \mathbf{Z}_{l,ij}} = \frac{\partial \mathbf{H}_{\mathrm{L,i}}}{\partial \mathbf{Z}_{l,ij}} \cdot \mathbf{H}_{\mathrm{O,LNA}} + \mathbf{H}_{\mathrm{L,i}} \cdot \frac{\partial \mathbf{H}_{\mathrm{O,LNA}}}{\partial \mathbf{Z}_{l,ij}}, \quad \text{for the voltage, and} \tag{3.23}$$

$$\frac{\partial \mathbf{H}_{\mathrm{L,LNAc,ind}}}{\partial \mathbf{Z}_{l,ij}} = \frac{\partial \mathbf{H}_{\mathrm{L,LNAv,ind}}}{\partial \mathbf{Z}_{l,ij}} \cdot \mathbf{Z}_{\mathrm{eqLNA1}}, \quad \text{for the current sources.} \tag{3.24}$$

3.3.3 Downstream Noise Gradient

Finally, we see that the transfer function of the downstream noise $\mathbf{H}_{\mathrm{L},\tilde{n}}$ is not affected by any of the derivations above under the unilateral assumption. Its gradient is zero, no matter the matching network or the relay loads.

Chapter 4

Problem Statement and Optimization Methods

This section analyzes the problem of optimization.. Although the thesis does not look into finding the optimal solution, different optimization strategies must be introduced and compared, as the utility function is not trivial and the differences are severe. We show the advantages and disadvantages of each strategy. If it is not specific mentioned, we use a 2x2 MIMO system with one receive antenna per user and three relays, as shown in Figure 2.2 as our baseline. The relays in this system will be lossless, which is to say the impedances will be purely imaginary.

4.1 Utility Function

As the aim for wireless communication networks is to maximize the achievable rates, we use the formulas derived in Section 2.4, which describe the rates for each transmit-receive pair. In order to get an utility function from the achievable rates, we take the vector of achievable rates $\mathbf{r} = \begin{bmatrix} r_1 & r_2 & \cdots & r_N \end{bmatrix}^T$ from Equation (2.57).

To optimize the rates, different approaches are possible:

- Optimize the minimum rate, or $\max(\min(\mathbf{r}))$ (maxmin), and
- Optimize the mean rate, or $\max(\sum(\mathbf{r}))$ (maxsum)

This is done using the LP-norm ($||\mathbf{r}||_p$) [7, p.853]. By setting $p = -\text{Inf}$, the "maxmin" method is achieved. Setting $p = 1$ applies the "maxsum" method. For all values in between, the utility function tends to optimize the sum and the minimum value respectively. In the following, we restrict ourselves to the "maxsum" method. The other methods easily can be applied and will lead to similarly good results without loss of generality.

4.1.1 Convexity of the Utility Function

In the following we analyze the convexity of the utility function. This is done because the choice of the optimization method depends on the shape of the utility function. In the case of a concave utility function, a normal gradient search is sufficient to provide good results.

We analyze the utility function at different input values for the passive relays. It is clear that the function (dramatically) changes for every channel realization. Figures 4.1 and 4.2 show two different channel realizations for the same input power and the same domain of two passive impedances.

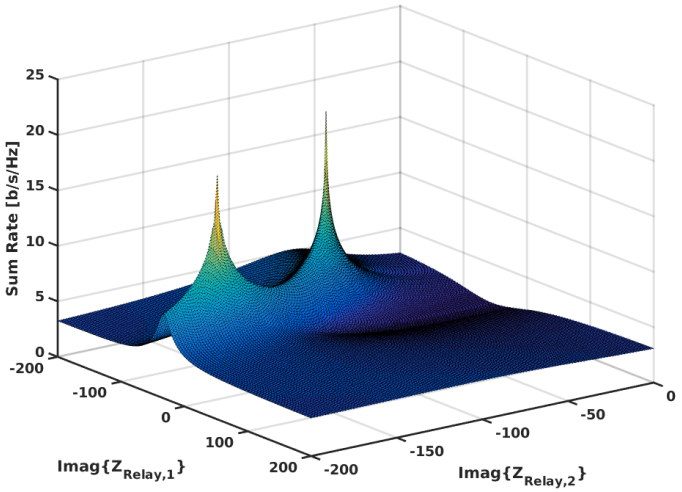

Figure 4.1: The utility function for a specific channel realization.

For the domain of the relay values showed in Figure 4.1, two local maxima can be found with immensely higher sum rate values. On the other hand, the utility function in Figure 4.2 shows only one local maximum with such a huge performance difference.

4.1.2 Dependency on the Input Power

We now analyze the utility function for different input powers. In Figure 4.2 and Figure 4.3 we see the same channel realization for two different input powers.

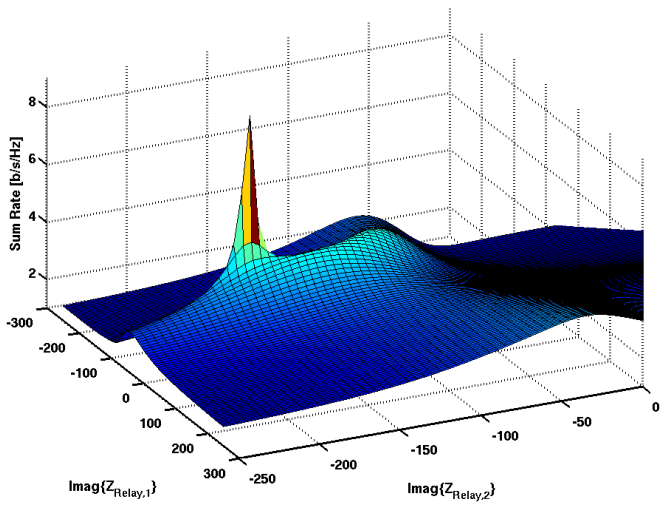

Figure 4.2: The utility function for another specific channel realization and a high input power level.

We observe that the optima in Figure 4.2 and Figure 4.3 lie at different impedance values for the relays, therefore we can conclude that an optimal solution for one

input power does not necessarily lead to a good solution for a different input power solution.

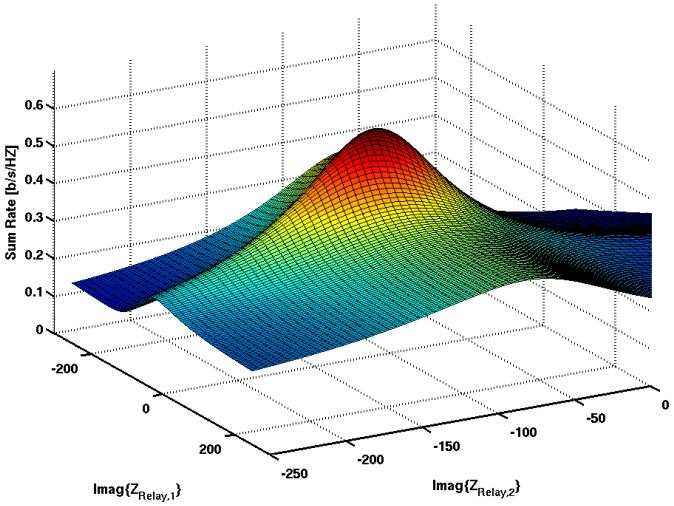

Figure 4.3: The utility function for the same specific channel realization as in Figure 4.2 and a moderate input power level.

4.1.3 Difference in Local Optima

Finally, we look at all local optima we expect to encounter. We see in Figure 4.1 that if we achieve the local optimum at the left, the performance will be nearly the same as with the local optimum at the right. However, in Figure 4.4 we see the differences of the local optimum at the right with above 18 [b/s/Hz] severely higher than the local optimum on its left with around 8.5 [b/s/Hz]. Therefore, we cannot simply run the optimization with one initialization, but instead we need multiple initializations to be sure that we have not missed a severe maximum.

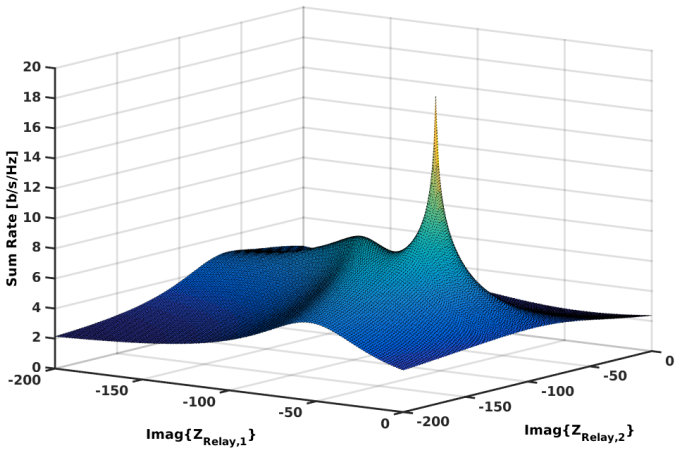

Figure 4.4: The utility function for a specific channel realization.

4.1.4 Complexity of the Problem

As we will discuss different optimization approaches in the following sections, we give a short description of the complexity of the problem here. For each relay we use, we will have one variable (N_{Rel}), if we restrict the relays to the imaginary domain. Allowing the relay to become lossy and therefore allowing the impedance to be complex, the number of variables doubles.Further, for each receiver branch or receiver antenna, we have a reciprocal (lossless) matching network (see Section 2.2.2), which must be optimized. Therefore we have three elements per branch: $3 \cdot N_{\mathrm{R}} \cdot N_{\mathrm{Rx}}$. For a four-user MIMO system with two receiver antennas and five lossy relays per user, this would lead to a problem of size $N_{\mathrm{var}} = 2 \cdot 4 \cdot 5 + 3 \cdot 4 \cdot 2 = 64$. As mentioned in the beginning of this chapter, we look at a 2x2 MIMO system with one receiver antenna and three lossless relays. The complexity of this system is therefore $N_{\mathrm{var}} = 1 \cdot 2 \cdot 3 + 3 \cdot 2 \cdot 1 = 12$.

4.2 Gradient Search

Despite our large number of variables and the non-convexity of the utility function, the first approach remains a gradient search. Figure 4.5 shows the typical behavior of the gradient search versus the iteration steps. In the following, different methods are described for improving the algorithm.

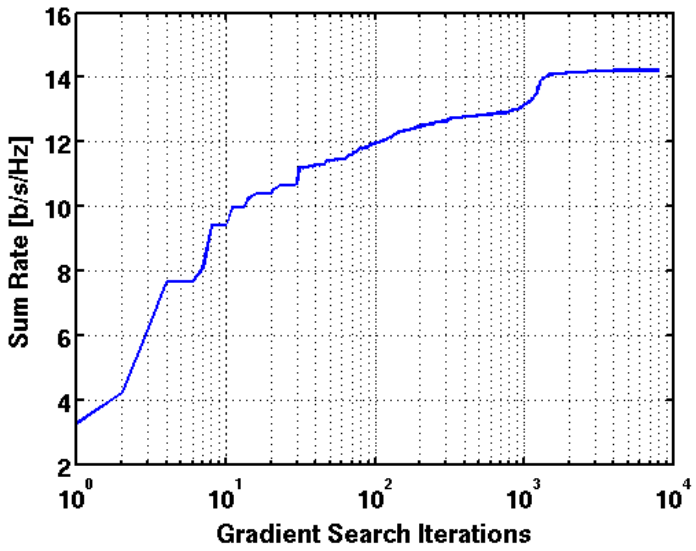

Figure 4.5: The sum rate over the gradient search iterations.

From Figure 4.5 it is obvious, why the method of gradient search is used despite the non-convexity of the problem: the rate is tripled after seven steps, and after 100 steps the rate is improved by a factor of four. After, only small improvements can be achieved, which leads to the assumption that a sufficiently good local maximum can be found very quickly. If, we assume that after such a smaller number of steps, no good result can be achieved, the initial value was poorly chosen. In those cases different initializations might yield to better results. This is also shown in the following section.

4.2.1 Choice of Initial Values

We try to overcome the unpleasant properties of the problem with a larger number of initial values. With this strategy the gradient search approach tends more towards a grid search optimization method. The gradient search routine itself is then used as a refinement step of the grid search.

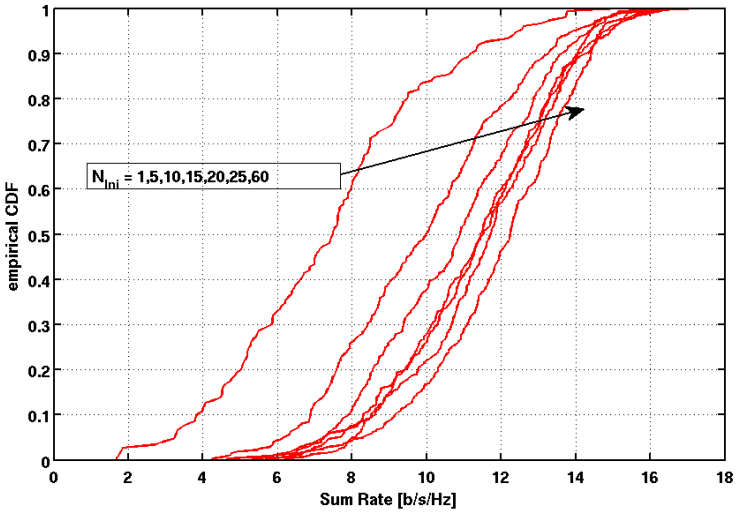

Figure 4.6: Comparison of the number of initial values used.

Figure 4.6 shows the empirical CDFs of the optimized sum rate for different numbers of initializations. The initial values were drawn uniformly at random for $Z_{\mathrm{Rel}}[i] \in [-600, 600]j, \quad \forall i \in [1, N_{\mathrm{Rel}}]$.

It is obvious that larger numbers of initializations yield better the result. However, even with 25 and 60 initializations, improvement is still immense. This shows that the number of initializations must be larger than twice the input vector length. A good tradeoff between decent optimization and comparably small run times is achieved by a choice of four times the input vector length.

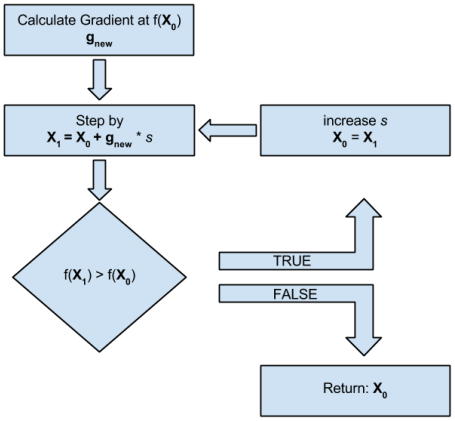

Figure 4.7: Schematic of the adaptive step size algorithm.

4.2.2 Adaptive Step Size

The performance of the gradient search routine is improved by the use of adaptive step sizes. For each calculated gradient, the step taken into the direction of the gradient is increased until the new rate value is smaller than the previous calculated value as shown in Figure 4.7. Therefore the number of time-expensive gradient calculations is reduced immensely.

4.2.3 Conjugate Gradient

As the gradient search performance still requires too many iterations, further improvements are made. The shape of such complex problems can — in some cases —

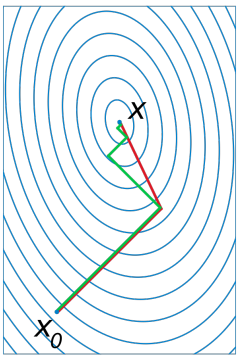

Figure 4.8: A comparison of the convergence of gradient descent with optimal step size (in green) and conjugate vector (in red) for minimizing a quadratic function associated with a given linear system[13].

have the shape of a crest as shown in Figure 4.8. In these a poorly chosen initial value causes the gradient search routine to jump around the optimum, without improving. Conjugate gradient routines like "Fletcher-Reeves" or "Polak-Ribière" lead to faster convergences, as they weight the gradient by the previous gradient and a weight factor β.

Like Polak-Ribière, the Fletcher-Reeves method updates the conjugate direction according to

$$\mathbf{s}_n = \mathbf{g}_n + \beta_n \cdot \mathbf{s}_{n-1}, \tag{4.1}$$

where $\mathbf{g}$ denotes the gradient. The conjugate direction $\mathbf{s}$ is then used to perform the conjugate gradient search. Polak-Ribière and Fletcher-Reeves differ in the way they calculate the weight factor β.

Fletcher-Reeves

For the Fletcher-Reeves method, β is calculated according to [14]

$$\beta_n^{FR} = \frac{\mathbf{g}_n^T \mathbf{g}_n}{\mathbf{g}_{n-1}^T \mathbf{g}_{n-1}}. \tag{4.2}$$

Polak-Ribière

For the Polak-Ribière method, β is calculated according to [15]

$$\beta_n^{PR} = \frac{\mathbf{g}_n^T \left(\mathbf{g}_n - \mathbf{g}_{n-1}\right)}{\mathbf{g}_{n-1}^T \mathbf{g}_{n-1}}. \tag{4.3}$$

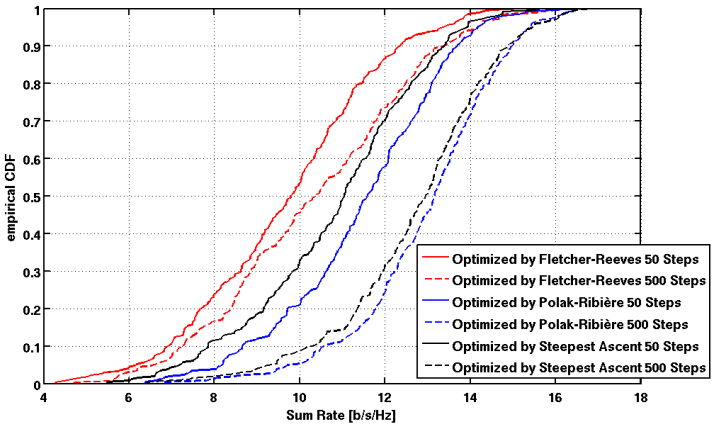

Figure 4.9: Comparison between Steepest Ascent, Polak-Ribière, and Fletcher-Reeves.

In Figure 4.9 the pure gradient search (steepest ascent) method is compared to the methods of Fletcher Reeves and Polak-Ribière. The Figure shows both the optimization after 50 iterations (solid lines), representing which method optimizes the problem the quickest, and after 500 iterations, representing which routine might be disrupted by the shape of the problem.

We can see that Fletcher-Reeves is not well suited for our kind of optimization problem. Polak-Ribière is better, outperforming the standard gradient search method at 50 iterations and slightly better after 500 iterations.

4.3 Heuristic Optimization Algorithms

Due to the non-convexity and out non-trivial optimization problem, we further analyze some heuristic optimization methods. In the following, three heuristic algorithms are introduced and analyzed for their performance.

4.3.1 Simulated Annealing

Simulated Annealing was developed to exploit the deep and useful connection between statistical mechanics — the behavior of systems with many degrees of freedom in thermal equilibrium at a finite temperature — and multivariate or combinatorial optimization — finding the minimum of a given function depending on many parameters [16]. In this thesis, Simulated Annealing was chosen as it is a method for solving optimization problems of multivariate optimization. The Algorithm used in this thesis is a build-in function of MATLAB. A description can be found on the MathWorks homepage [17].

Figure 4.10 shows the performance of Simulated Annealing algorithm dependent on the choice of numbers of initializations (red curves). Again, we see, that more initializations yield better sum rates. However, we also see that, even with 60 initializations, Simulated Annealing leads to a worse result than the sum rates achieved by steepest ascend (black dashed curve) and Polak-Ribière (blue dashed curve).

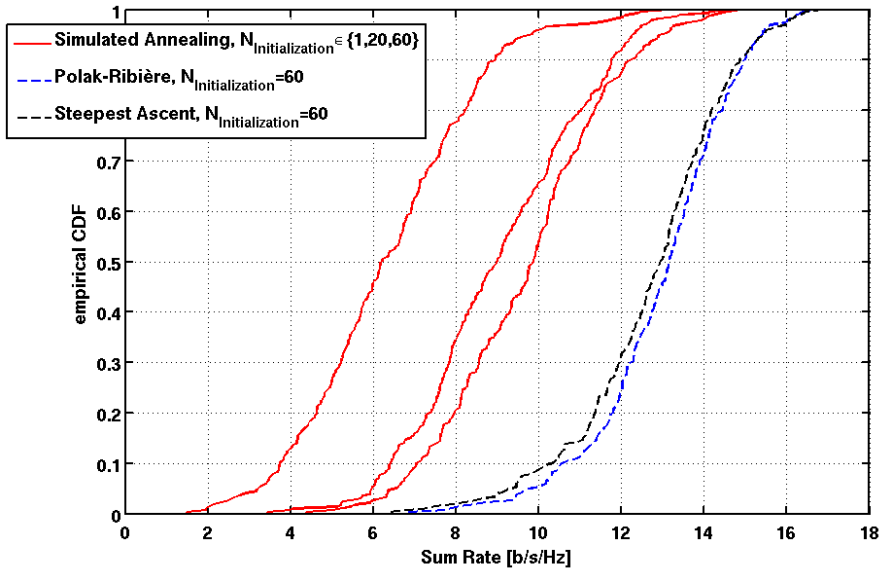

Figure 4.10: Comparison of the Simulated Annealing algorithm for different number of initializations (increasing from left to right) and the results from "Polak-Ribière" and "Steepest Ascent" gradient searches.

4.3.2 GlobalSearch

The other two heuristic optimization algorithms are GlobalSearch (GS) and MultiStart (MS). They are very similar to each other, the only difference is the choice of starting values. MultiStart requires the number of initialization values, while GlobalSearch generates trial points on its own [18]. GlobalSearch — the optimization function we analyze — is based on the MATLAB built-in function *fmincon*. Figure 4.11 shows the schematics of GS and MS.

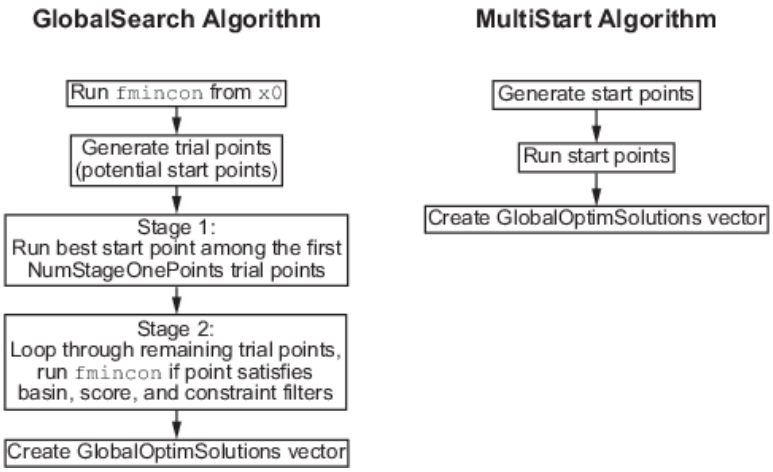

Figure 4.11: Schematics of the GlobalSearch and MultiStart algorithms [18].

Figure 4.12 shows the performance of GlobalSearch (red curve). We see that it has almost the same performance as the conjugate gradient method by Polak-Ribière with 60 initializations (blue curve). Compared to gradient search methods

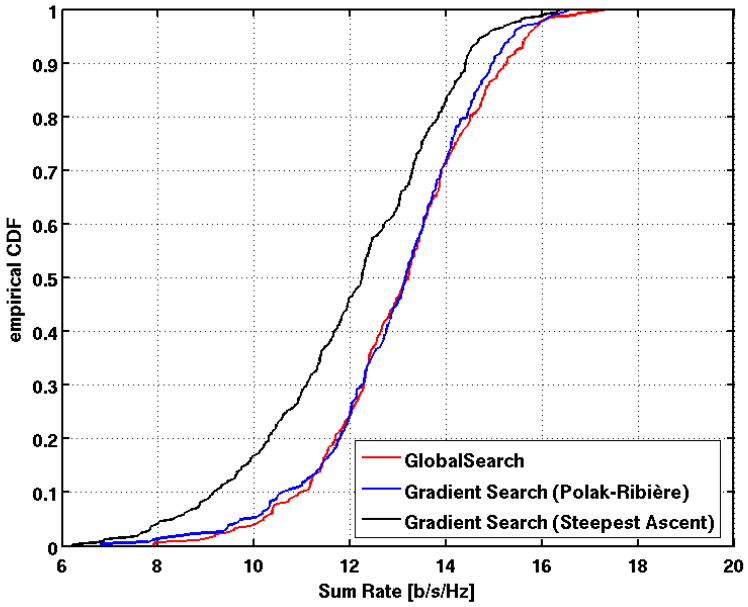

Figure 4.12: Performance of the GlobalSearch algorithm in comparison to the previous results.

GlobalSearch is less dependent on the initial value. Therefore we choose very large values for the relay loads ($\mathbf{X}_{\mathrm{Rel}} = 1000j$), to simulate an open circuited antenna and therefore no coupling.

4.4 Further Algorithm Improvements

4.4.1 Optimization of the Interference Function

A further approach optimizing the gradient search routine is a good initial guess. The problem of sum rate maximization is reduced to the elimination of interference. Therefore the number of variables can be reduced by a factor of two thirds for the matching network, as the interference function from Equation (2.16) — even after multiplication with the spatial channel transfer function (2.2) — only requires the input impedance of the matching network. This reduced problem has size of $N_{\mathrm{var}} = 2 \cdot N_{\mathrm{Rel}} + 2 \cdot N_{\mathrm{R}} \cdot N_{\mathrm{Rx}} = 2 \cdot 4 \cdot 5 + 2 \cdot 4 \cdot 2 = 56$ for the same settings as above. The factor 2 from the matching network variables comes from the fact that with pure imaginary elements in the matching network any complex value of the equivalent input impedance can be achieved.

Figure 4.13 shows the performance of the steepest ascent algorithm, with the pre-optimized initial values (three red dotted curves on the left). We see that, using the five best pre-optimizations leads to a performance almost as good as initializing the algorithm with 60 random vectors (red solid curve). To push the optimization even further, we can combine these two techniques and take the best optimization from the five best pre-optimized initial values and 55 random initial values (red dotted curve on the right). This leads to a 0.5 [b/s/Hz] improvement at the mean and a 1.5 [b/s/Hz] improvement for the lowest 10% of the rates compared to only considering random values.

Applying this to the method of Polak-Ribière (blue dotted curve), however, does

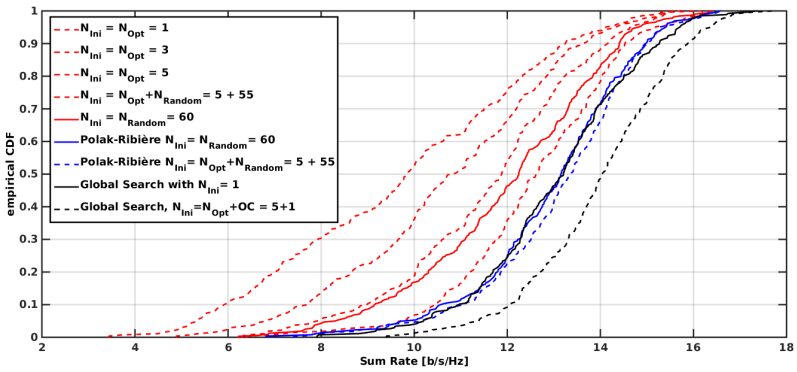

Figure 4.13: Comparison of the number of initial values used with different pre-optimized intial values.

not improve the results as much as we did with the steepest ascent method. A sum rate of only about 0.1 [b/s/Hz] higher is achieved by using pre-optimized initial values in combination with the method of Polak-Ribière.

Finally, this method is applied to the heuristic GlobalSearch routine. As mentioned in Section 4.3.2, GloablSearch is less dependent on the initial value and therefore, the initial value is chosen to be open-circuited for the relays. With five optimized initial values plus the standard open circuit initial value, an improvement of almost 1.0 [b/s/Hz] can be achieved (black dotted curve) compared to initializing only by the open circuited value (black solid curve).

4.4.2 Post Refinement of GlobalSearch by Gradient Search

When the problem of gradient search is that it may run into non-optimal local maximas, the questions for heuristic optimization methods are: "How good are the results after all?" and "Can they be improved any further?"

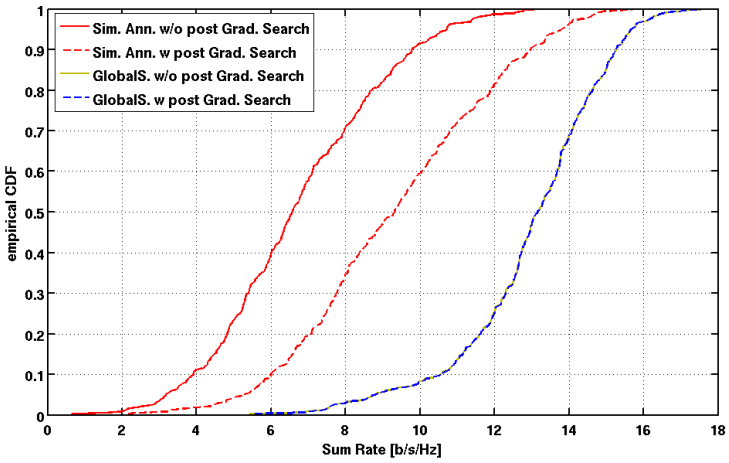

Figure 4.14: Comparison the heuristic optimization methods with and without a post refinement by gradient search.

The approach to finding the answers is to use the gradient search routine on top

of the heuristic optimization as a refinement. Figure 4.14 shows the performance of the Simulated Annealing and the GlobalSearch algorithms (solid red and solid yellow curves). The dashed lines show the result when gradient search was added on top of the heuristic optimization (red dashed for Simulated Annealing and blue dashed for GlobalSearch). This shows that the poor results of the Simulated Annealing algorithm do not lead to good initial values for the gradient search. After the refinement, the performance is about 5 [b/s/Hz] worse than the performance of GlobalSearch. Second, it shows that the performance of GlobalSearch is quite good, as any post-refinement of gradient search *does not lead to any significant improvement*.

4.4.3 Stepwise Optimization

In the previous Sections, we saw the performance of different methods for three relays per user. The number of relays was kept small for the analysis of the algorithms to avoid complexity effects reducing the performance. Increasing the number of relays might result in worse sum rates, as the complexity of the system correlates with the number of initial values required to achieve similarly good results. Then the run time of the optimization routine must be increased or the precision is decreased. Therefore we now look at the performance of the optimization and how it can be pushed. For the results shown below, the number of relays were increased to seven, if not mentioned specifically.

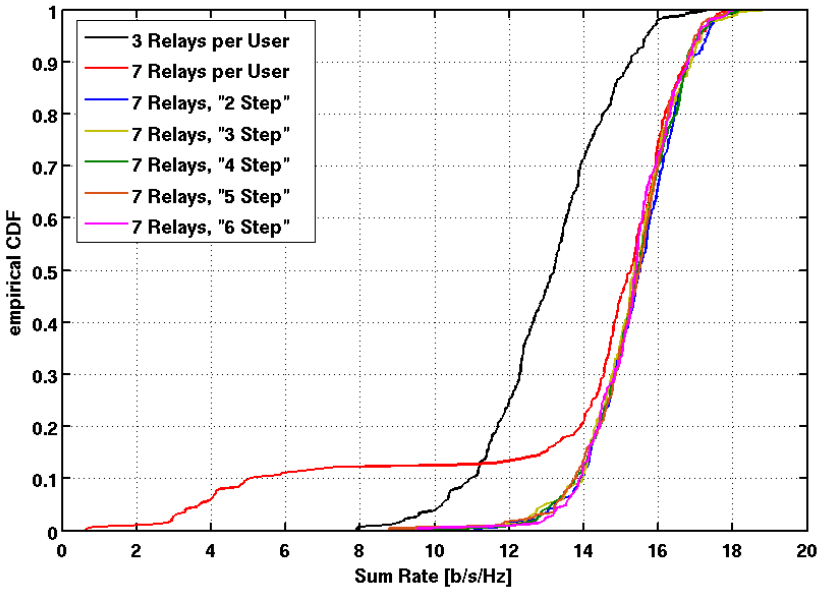

Figure 4.15: Comparison of the number of step wise optimization.

In Figure 4.15 we see the performance of the GlobalSearch algorithm optimizing a 2x2 MIMO system with seven relays and one receiving antenna per user (red curve). The black curve shows the performance of the algorithm optimizing only three relays per user (c.f. red curve in Figure 4.12). This should be the lower limit of the red curve, as one solution for seven relays is to optimize only three of them and open circuit the remaining four. However this is only the case for about 85% of the cases — the lowest 15% actually lead to worse solutions than only optimizing three relays. This shows that GlobalSearch optimization might not perform very

well on larger problems — reducing the size of the problem results in a better sum rate.

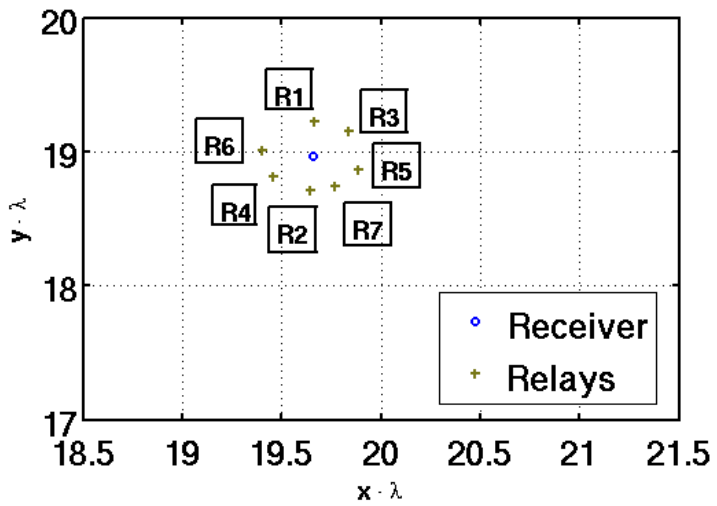

Figure 4.16: Example of choosing the relays for stepwise optimization.

One approach to prevent GlobalSearch from running into a low rate is to reduce the number of relays for optimization and increase them stepwise. The blue curve shows the result of the optimization, when GlobalSearch is allowed to optimize only two relays. Once finished, two additional relays are considered so that in total four relays per user are optimized. This is repeated until the total number of relays is reached (in this case four times, $N_{\mathrm{Rep}} = \lceil \frac{N_{\mathrm{Relays}}}{N_{\mathrm{Step}}} \rceil = \lceil \frac{7}{2} \rceil = 4$). Hereby, the first relay is chosen at random. For the following relays, the algorithm always takes the next free relay across the receiver. Figure 4.16 shows an example of how the relays would be chosen for this setting. The stepwise optimization method leads to a tradeoff between the precision of the routine and the run-time, as a smaller number of relays per step (N_{Step}) will likely lead to a better result, but also to a larger number of repetitions and therefore will take much longer ($\approx N_{\mathrm{Rep}} * \mathrm{T}_0$, for T_0, the time for one optimization).

In Figure 4.15, the yellow curve shows the optimization for a stepwise increment of $N_{\mathrm{Step}} = 3$ (denoted in the legend as "3 Step"). Therefore we use $N_{\mathrm{Rep}} = 3$ as our baseline. For $N_{\mathrm{Step}} = 4$, $N_{\mathrm{Step}} = 5$, and $N_{\mathrm{Step}} = 6$ (with each $N_{\mathrm{Rep}} = 2$), we find almost to the same result. Also none of the stepwise optimization has a significant low-rate outlier, therefore we can say that the outliers from direct optimization can be avoided when a single repetition is added.

A second approach is to optimize one user and its relays for each step. This reduces the size of the problem to $N_{\mathrm{R}} \cdot N_{\mathrm{Rx}} + N_{\mathrm{Rel}}$ for each optimization step. The number of optimization steps is increased by N_{R}. Additionally, after optimizing each user, a final step might be included in which the whole system is refined, which leads to a number of $N_{\mathrm{Rep}} = N_{\mathrm{R}} + 1$ repetitions. Figure 4.17 shows the performance of this method for a 2×2 system with three relays per user. The blue solid curve denotes the performance of optimizing the system directly. The red solid curve shows the performance of optimizing each user on its own and additionally optimizing the whole system in a refinement step after. Optimizing each user in advance of optimizing the whole system, leads to a slight improvement, even for this small system.

For both cases — the user stepwise optimization and the relay stepwise optimiza-

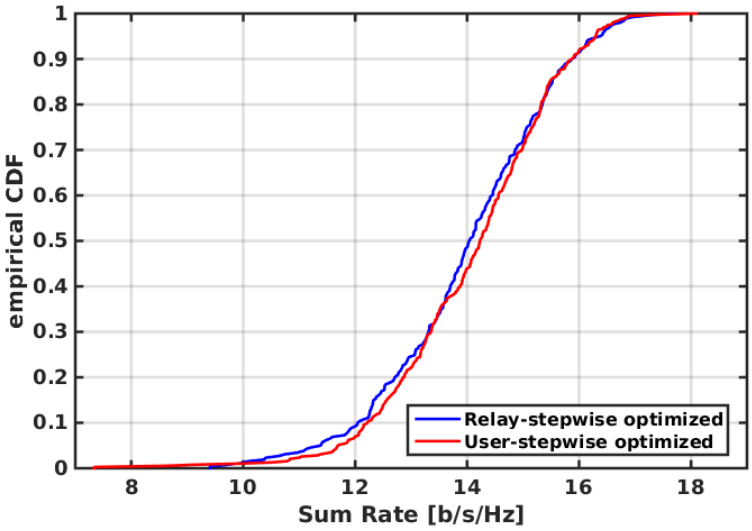

Figure 4.17: Comparison of optimizing the relays stepwise versus optimizing each user per step.

tion — a lower sum rate limit constraint is set after each step. With this inequality constraint, the heuristic algorithm is prevented in running into a lower rate than it had in the previous step.

Chapter 5

Simulation Results

This section discusses the results we found in this thesis. The performance of the optimization routine is shown for different settings, that is for different numbers of relays, receiving antennas per user, users, relay placings, and input powers. Unless otherwise stated, we use the same settings as in Section 4: we look at a two-user system with one receiver antenna and three relays per user, as shown in Figure 2.2. The relays in this system are lossless, meaning that impedance will be pure imaginary. Additionally, we only consider noise contributions of the circuitry after the LNA, or only downstream noise (c.f. Equation (2.33)). Therefore, because of the unilateral assumption, the noise contribution will be i.i.d. and independent of the matching network or the relays. Hence, the optimization algorithm only adapts to the signal and the interference.

5.1 Introduction of Measures for Comparison

In order to rate the results on quality, their performance will be compared to classical interference-eliminating methods such as TDMA. Additionally, improvements from the uncoupled case will be given as well as theoretical performance limits, in order to see how much the performance can be pushed. In the following, the rates to which the optimization is compared are introduced.

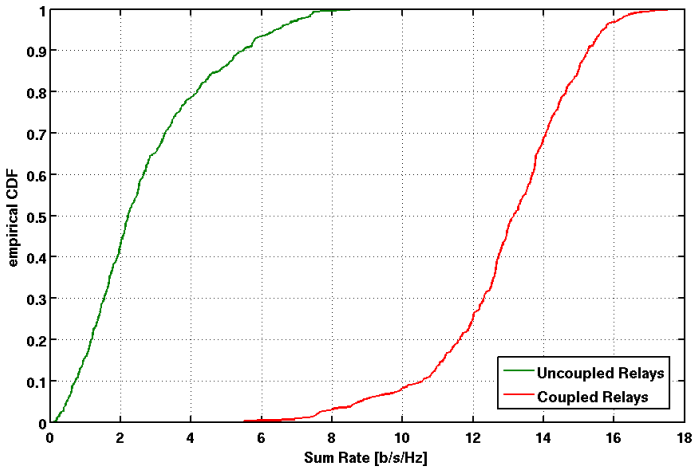

Figure 5.1: Comparison of uncoupled relays and optimized coupled relays.

5.1.1 Uncoupled Relay Rates

One of the logical comparisons for the use of loaded antennas is the same setting without any coupling among the relays. Logically, the "uncoupled relays rate" —- later sometimes also only "uncoupled rate" — should be smaller than including the relays and adapting their impedances to our needs. If no higher rate can be achieved, the whole idea of using passive relays would fail. Hence, the uncoupled relay rate serves as a lower limit which should be achieved.

In Figure 5.1, the green solid line shows the performance if no coupling among the relays and receivers exists. It is clear that the rates including relay coupling (red solid line) are much larger. Therefore, this method is suitable for improving achievable rates.

5.1.2 TDMA Rates

In the next step, the optimized rates are compared to the TDMA rates for the equivalent setup. Therefore, the relays are again assumed to be uncoupled from the receivers and the transmit/receive pairs are assumed to divide time equally among themselves for transmission. For this calculation the formulas from Equations (2.61) and (2.62) are used.

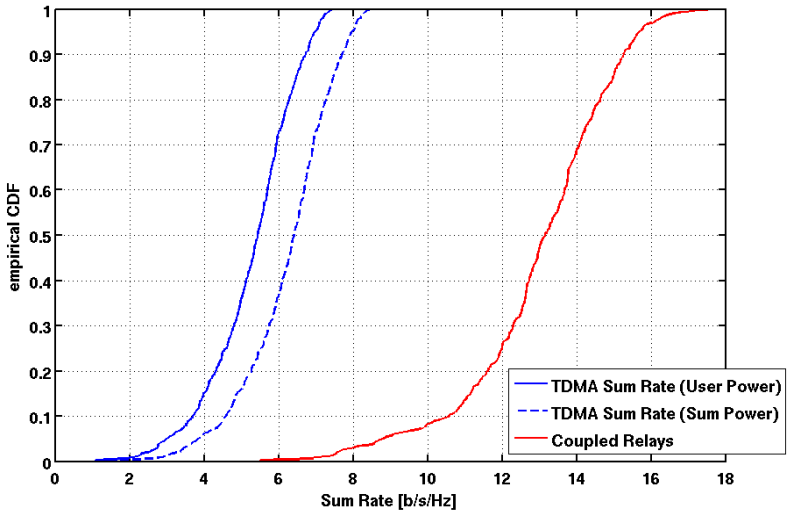

Figure 5.2: Comparison of the TDMA rate and optimized coupled relays.

In Figure 5.2, the blue solid line shows the performance if TDMA is applied under the user-power constraint (i.e. the limit of the transmit power is given for each user and is therefore the same for each user as in the coupled relay case) and the relays are uncoupled from the receivers. The blue dashed line shows the performance of TDMA under the sum power constraint (i.e. the limit of the transmit power is given by the total transmit power and therefore the power per user in TDMA is N_{User} times the power per user in the coupled relay case —- here two times). As before, the rates including relay coupling (red solid line) are much larger than those without any coupling and TDMA. Of course, this comparison is more dependent on the choice of the settings —- especially the choice of the number of transmit-receive pairs —- and we will see different behaviors in the following sections.

5.1.3 Noise-free Rates

As we are addressing the problem of interference, a good measure is the noise-free rate (SIR-rate). It is calculated similarly to the SINR-rate, however it only considers the interference and not the noise (c.f. Equation (2.60)). As written in the previous chapters, in high-SNR regimes, the interference is the main diminishing factor for achievable rates (c.f. Section 2.4), and the SIR-rates will give an indicator of how well the relays and matching network are optimized. Example curves of the SIR-rates (blue dashed lines) can be seen in Figures 5.7 to 5.9.

5.1.4 Relays as Full-Cooperation Receivers - Limit

The remaining two function against which the rates after our optimization algorithms are compared give limits on how good the method of loaded antennas can potentially be. The first approach is to consider relays as full-cooperation receivers, which are widely spread. Hence they experience no coupling among themselves and are spatially uncorrelated. The number of observations the receiver has on the incoming signals is increased to $N_{\mathrm{Rx}} + N_{\mathrm{Relays}}$. As we choose the number of relays to be larger than the number of interferers in most cases, this method will lead to an interference-free connection.

The performance of the full-cooperation relays can be seen in Figure 5.3 (black solid curve). At the median it is almost 2 [b/s/Hz] higher than the optimized rate of the passive coupled relays. For the best 10% of cases, this is reduced to 1 [b/s/Hz] or lower; for the worst 10% of cases, it lies between 2.5 [b/s/Hz] and 4.7 [b/s/Hz].

5.1.5 Multiport Matching - Limit

It has been shown that the multiport matching is the optimal setting for a matching network, without considering any relays [2]. For our comparison with the coupled relays, the relays are assumed to be full-cooperating receiver antennas. However,

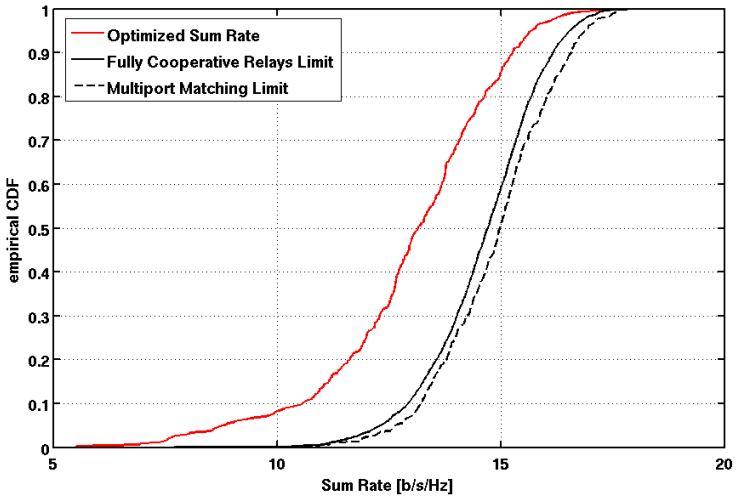

Figure 5.3: Comparison of the full cooperation relay rates, multiport matching rate and optimized coupled relays rate.

the placement of the relays remains the same, so no widely spread receivers are assumed. The number of observations for each receiver, is $N_{\mathrm{Rx}} + N_{\mathrm{Relays}}$ again. Hence, it can be expected that the new rate is higher than the optimized coupled

relays rate. In Figure 5.3 and the following, this limit is shown by the black dashed line.

5.2 Relay Placing

Before analyzing the solver with different settings, we discuss the placement of relays around a receiver in more detail. Figure 5.4 shows the criteria by which the relays are placed. The red solid circle with radius d_z denotes a zone around the

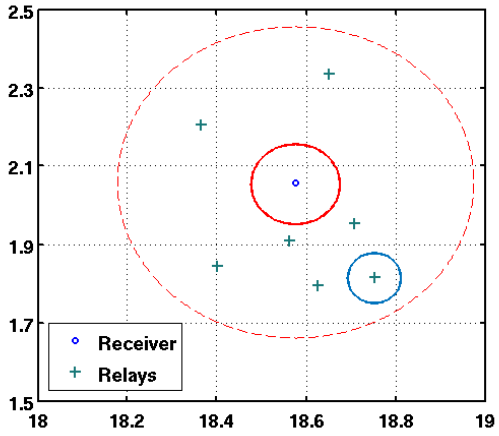

Figure 5.4: Placing the relays around a receiver uniformly distributed on a disc.

receiver in which no relays must be placed. The red dashed line shows the maximum distance at which the relays may be placed away from the receiver. Within those two lines, the relays are thrown uniformly at random. The blue circle with radius d_{Relay} around the relay at the right bottom denotes a zone in which no other relay may be placed, or the minimum distance between each relay. If there is a violation of the relay distances, all relays are thrown again.

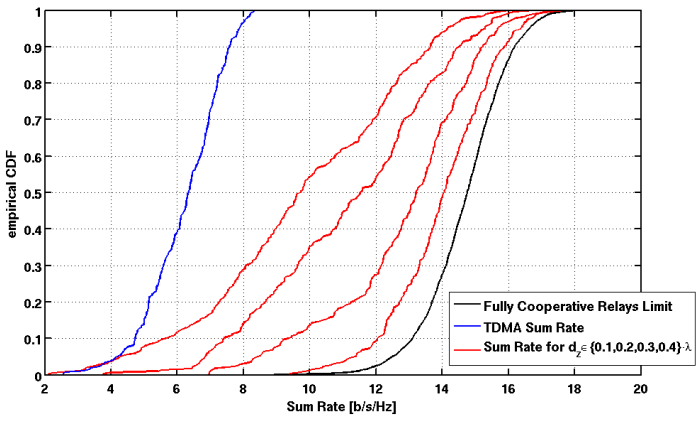

Figure 5.5: Optimized Sum Rates for different minimum distances between receiver and relays ($d_z \in \{0.1, 0.2, 0.3, 0.4\}$ from right to left).

The minimum receiver distance and the minimum relay distance might differ, but unless otherwise specified they are both assumed to be 0.1λ. With a smaller choice

of maximum distance, the relays can be placed more densely. When the maximum distance is set equal the minimum distance, the relays will be placed along the perimeter of a circle around the receiver.

Figure 5.5 shows the performance of the optimized sum rate for $d_z \in \{0.1, 0.2, 0.3, 0.4\} \cdot \lambda$ (red curves from right to left) and the same maximum distance. For all of the curves, the relays had the same minimum spacing of $d_{\text{Relay}} = 0.1 \cdot \lambda$. Obviously a higher rate can be achieved when the relays are closer to the receiver and thus the coupling is stronger. Even with a minimum distance of 0.4λ, the achievable rate is higher than the the TDMA rate (blue solid curve) under the sum power constraint.

5.3 Low SNR performance

First, we analyze the optimization algorithm at different SNR levels. Later we will only look at a high SNR level, as our aim is to minimize the interference. As we assume only downstream noise, the optimization algorithm can only change the signal and interference covariance matrices.

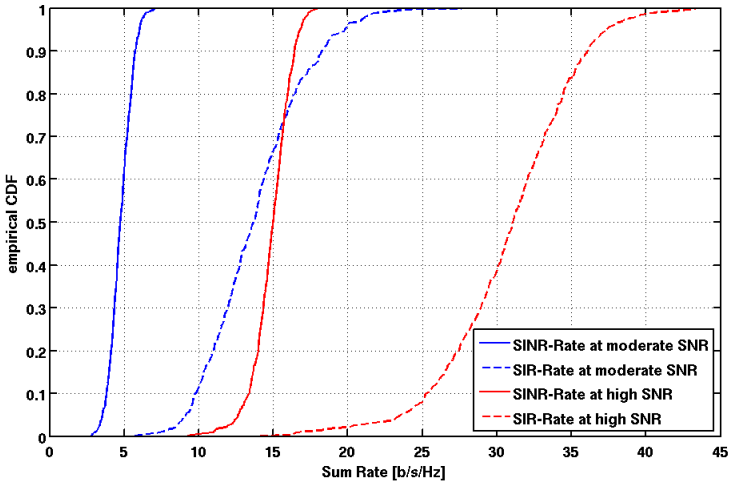

Figure 5.6: Comparison of the optimization algorithm at a moderate and high SNR level and the comparison to the noise free (SIR) rates.

Figure 5.6 shows the SINR- and SIR- rates at a moderate SNR level (blue curves) and at a high SNR level (red curves). As the achievable rate at a moderate SNR level (blue solid line) is less interference-driven and more noise-limited, the resulting SIR-rate (blue dashed curve) is also lower than the SIR-rate of the optimized achievable rate at a high SNR region (red dashed line).

This shows that, for the moderate SNR level, the optimization algorithm matches the values of the relays and the matching network in order to first amplify the signal and only second reduce the interference. For two users (as is here the case) the interference is increased at the same rate as the signal power (from moderate SNR to high SNR). If the optimization would have allowed the same reduction of the interference at the moderate SNR level, the SIR rates would have become equivalent.

5.4 Number of Relays for Eliminating Interference

In the following, the number of relays required for an interference-free connection is determined. For the following plots, the number of receivers is set to one ($N_R = N_{R_x} = 1$) in order to increase the performance of the solver (c.f. Section 4.4.3).

In the following sections the term "*interference-free*" will be used. This term indicates only reduced interference. Full interference elimination — as in a MIMO system with more receiver antennas than interferers — will not be reached. However, when the term is used the interference will be so low that the effect of noise will be an equivalent or even stronger diminishing factor.

5.4.1 One Interferer

To eliminate interference with two transmitters, two observations are normally required. Figure 5.7 shows the performance of a transmit/receiver pair with one interferer and $N_{\text{Rel}} \in \{1, 2, 3\}$ (red curves from left to right). It is clear to see, that

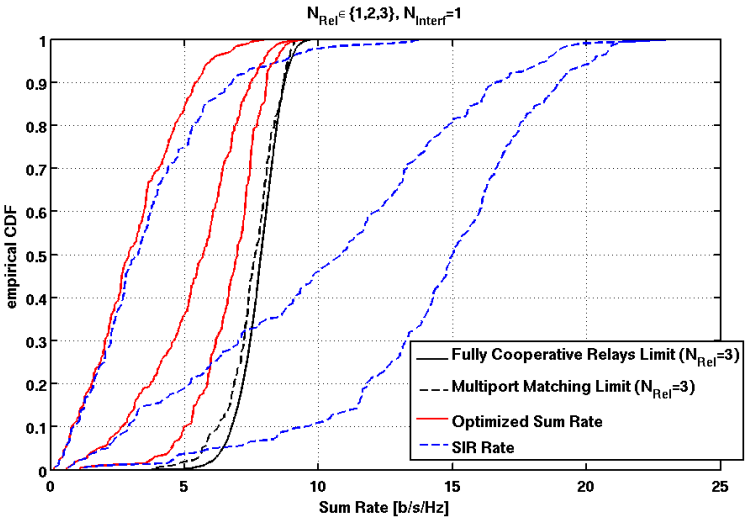

Figure 5.7: User rates for one interferer and one receiver with $N_{\text{Rel}} \in \{1, 2, 3\}$ (red and blue curves from left to right) and their theoretical limits (black curves).

higher the numbers of relays, yield better performance in the optimized system. The blue dashed lines show the rates considering only the SI-ratio (c.f. Equation (2.60)). The use of only one relay leads to an interference-free connection for only 10% of cases. Increasing the number of relays to two leads to an interference-free connection of almost 80% of cases. Achieving a noise-limited connection requires at least three relays per receiver in almost all cases.

5.4.2 Two Interferers

To eliminate interference with three transmitters, three observations are normally required. Figure 5.8 shows the performance of a transmit/receiver pair with two interferers and $N_{\text{Rel}} \in \{2, 3, 4, 5\}$ (red curves from left to right). As before, the blue dashed lines show the rates considering only the SI-ratio.

We see that, for two relays per user, the interference-limited rate behaves almost the same as the optimized achievable user rate. For three relays per user, some cases lead to an interference-free connection. Only in the case of five relays per user can over 90% of cases be driven into a low-interference state.

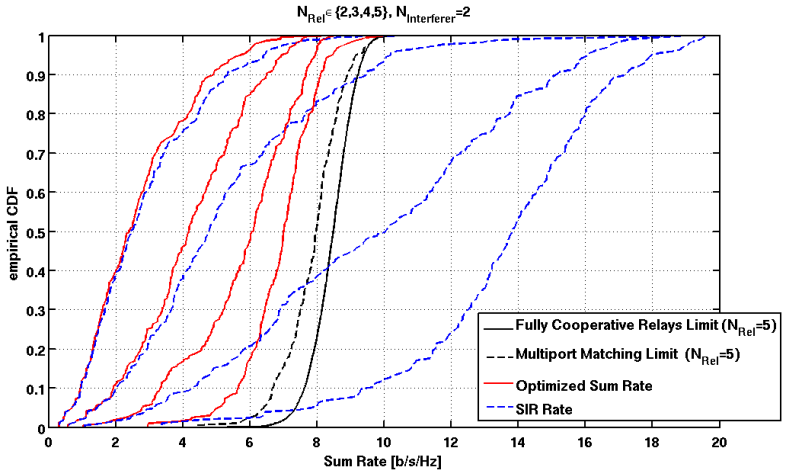

Figure 5.8: User rates for two interferers and one receiver with $N_{\text{Rel}} \in \{2, 3, 4, 5\}$ (red and blue curves from left to right) and their theoretical limits (black curves).

5.4.3 Three Interferers

To eliminate interference with four transmitters, four observations are normally required. Figure 5.9 shows the performance of a transmit/receiver pair with three interferers and $N_{\text{Rel}} \in \{4, 5, 6, 7\}$ (red and blue dashed curves from left to right).

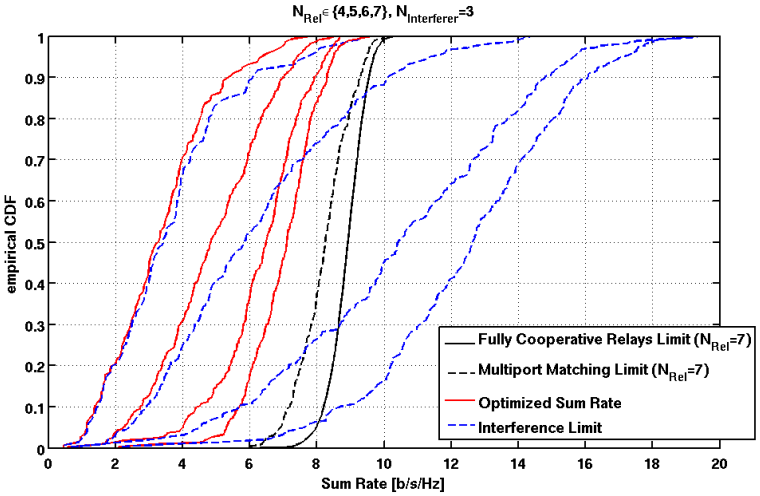

Figure 5.9: User rates for three interferer sand one receiver with $N_{\text{Rel}} \in \{4, 5, 6, 7\}$ (red and blue curves from left to right) and their theoretical limits (black curves).

We see that, for four relays per user, the interference-limited rate behaves almost the same as the optimized achievable user rate. For five and six relays per user, some cases lead to an interference-free connection. For seven relays per user, over 90% of cases can be driven into an low-interference state.

Comparing this to the previous results with one and two interferers, we can see that the number of relays required to eliminate interference does not grow linearly as with the use of fully cooperating receivers. It appears that it requires at least twice the number of interferers ($N_{\text{Rel}} > N_{\text{Interferer}} \cdot 2$) per user to overcome the interference.

5.4.4 Cooperative versus Non-cooperative Receive Antennas

In the following, we analyze what happens if the number of relays plus receiver antennas is kept constant. First, we analyze the case of one receive/transmit pair and three interferers, as this decreases the size of the problem by a factor of four. Behaviors like those in Section 4.4.3 are therefore less likely to occur.

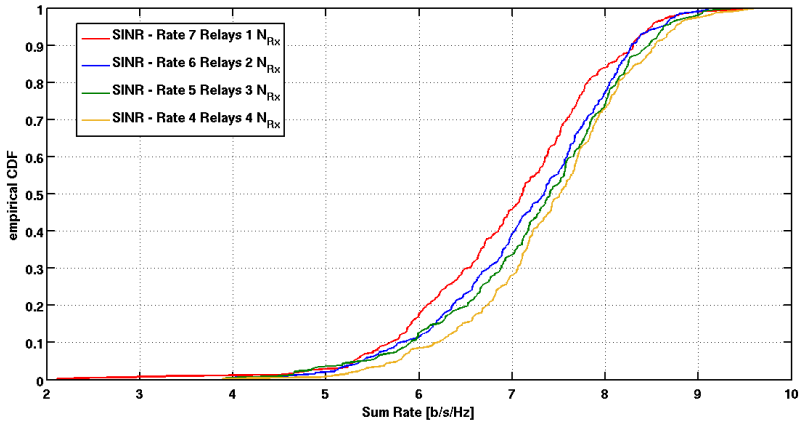

Figure 5.10: Comparison of constant $N_{\text{Rel}} + N_{\text{Rx}} = 8$, with $N_{\text{Rel}} \in \{4, 5, 6, 7\}$ and $N_{\text{Rx}} \in \{1, 2, 3, 4\}$ from left to right.

Figure 5.10 shows the performance with three interferers and one transmit/receive pair. Obviously in the case where four receiver antennas are used (yellow curve), the interference can be fully zero-forced and therefore it also shows the highest rate. However the performance is only 0.5 [b/s/Hz] smaller if seven relays and only one receive antenna are used (red curve) — even less for the values in between (blue and green curves). This shows that, with one additional observation and one fewer relay, the rate cannot be improved significantly. Therefore we can stick with

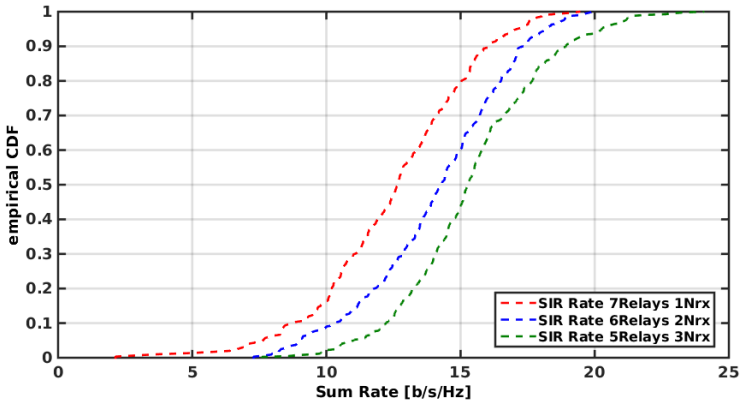

Figure 5.11: Comparison of constant $N_{\text{Rel}} + N_{\text{Rx}} = 8$, with $N_{\text{Rel}} \in \{4, 5, 6, 7\}$ and $N_{\text{Rx}} \in \{1, 2, 3, 4\}$ from left to right, showing only noise free rates.

a system that uses one receiver antenna and multiple relays, and can expect to perform similarly to a MIMO system with a sufficiently large number of receiver antennas to zero-force any interference.

Figure 5.11 shows the noise free, hence interference-limited rates for a constant number of relays and receivers. The SIR-rate for the receiver with four antennas is neglected, as the interference can be fully eliminated. Again, it can be seen, that the larger the number of receive antennas, the better the interference can be reduced. However, the differences are — as mentioned above — small. Therefore we can conclude, that a system can almost perform the same by increasing the numbers of relays, as it would increasing the number of receive antennas. Additionally, the problem complexity is kept smaller by using relays, as one receive antenna adds three variable by the matching network, but one relay only adds one variable for its load.

5.5 Four User System

In the previous sections, the requirements for a system with three interferers were given. Therefore in the following sections a full-four user system will be analyzed to determine whether the conclusions drawn from the previous sections are correct.

5.5.1 Prediction for four Users

Using the results shown in the previous section, the performance of a four-user system can now be predicted. A simulation of a four-user system with widely spread receivers should lead to the same results as would summing up the previous curves four times.

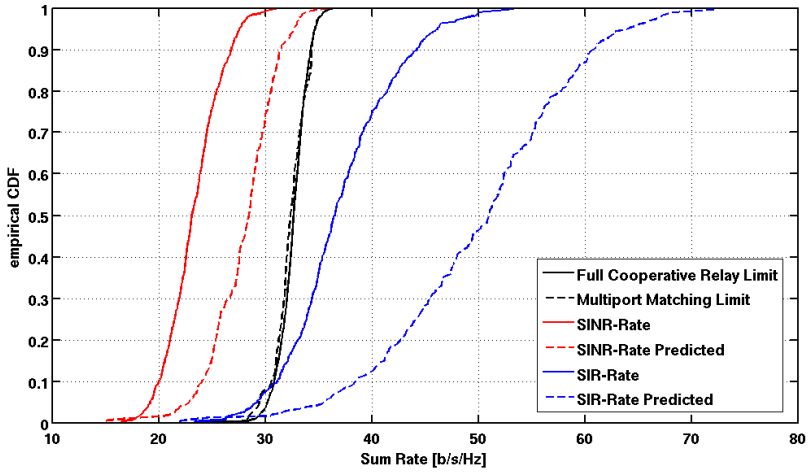

Figure 5.12: Plot of the 4 User System, with the predicted performance.

Figure 5.12 shows predicted performances (dashed lines) compared to simulated performances (solid lines). The rates of the simulated realizations are lower than the predicted behavior. For the simulation, the receivers were not placed widely apart, which is one reason for the lower rates as the non optimized coupling among receivers diminishes the performance. The second reason is, as mentioned above, the lower performance of the optimization algorithm with a larger problem. Still, we can conclude that the optimal solution must be between the solid and the dashed curves.

Additionally, the black curves give the theoretical limits of the sum rates. Because the predicted performance does not outperforme the theoretical limits, it follows that the optimal solution lies near the predicted performance.

5.5.2 Full Four-User System Performance

Finally we analyze the relay and matching network optimization of a four-user system. Two typical realizations and antenna placings can be seen in Figure 5.15. The achievable rates after optimization are analyzed in the following for such and other placings.

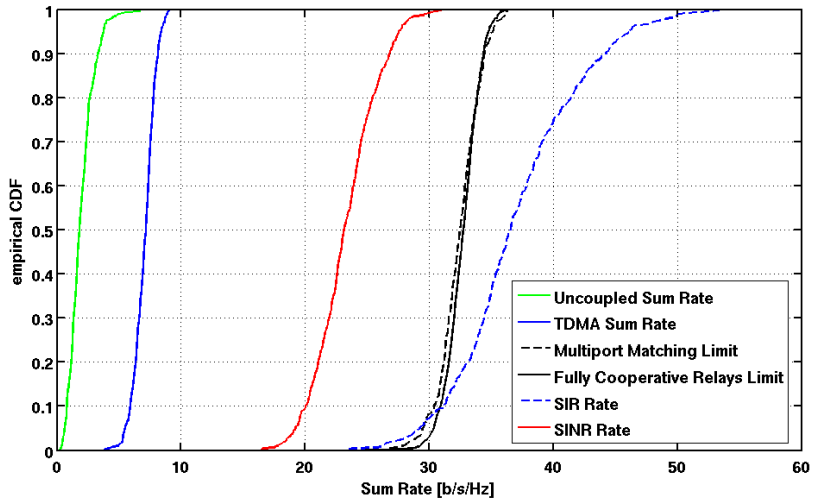

Figure 5.13: Sum rates of a 4 user MIMO system.

Figure 5.13 shows the sum rate of the optimized system (red solid curve) compared to the rates we introduced in the beginning of this chapter. We see that the uncoupled rate — in which each receiver has only one receiver antenna and no relays — and the TDMA rate (under the sum power constraint) are outperformed by far. Further, we see that the noise-free rate (dashed blue line) is always larger by at least 10 [b/s/Hz], which lets us assume, that the interference cancellation was performed well and that we are in an interference-free region for at least some users. The black curves denoting the fully cooperative relays limit and the multiport matching limit (dashed curve) are between 5 [b/s/Hz] and 10 [b/s/Hz] bits per second larger than the optimized sum rate. From Figure 5.9 we know that the limits are around 2 [b/s/Hz] larger than the optimized sum rate per user. This shows that, at the median for four users, the optimization algorithm performs almost as well as for one user, however the lower rates seem to suffer from poor optimization.

We saw in Figure 5.9 that it requires at least seven relays for one user to eliminate the interference from three users. Figure 5.14 shows the rates for each transmit/receive pair in red solid curves. Again, the black dashed curves denote multi-port matching rates, the green solid lines denote performance if the relays are uncoupled, and the blue solid line shows the TDMA rate for each user under the sum power constraint.

We observe that the uncoupled rate as well as the TDMA rate are outperformed by around 5 [b/s/Hz] for the three top users at the median. The lowest user, however, is — contradicting to the results from Section 5.4.3 — not interference-free for almost 50% of cases. For 10% of cases, it even shows worse performance than the TDMA rate. It seems, that this user is, for some realizations, blocked in order to enhance the other three users. This might be the optimal solution, but it might also be that the solver did not reach the best optimum.

To explore this a little bit further, Figure 5.15 shows typical placings when the

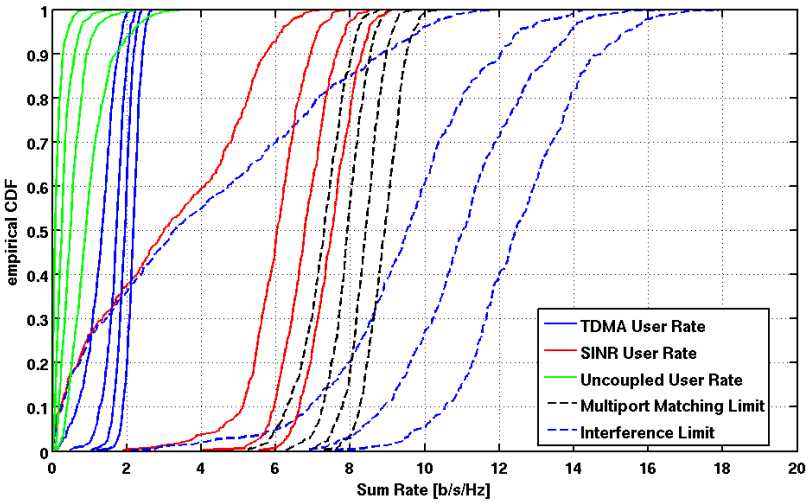

Figure 5.14: The user rates for four users with seven relays each.

minimum user rate could be improved strongly (on the left) and when the rate could only be improved a little (on the right). Both subplots show a field of size $2\lambda \times 2\lambda$. For the left subplot, the receivers have larger distances between them and the relays' belonging to the receivers can be easy distinguished — they are more or less nicely separated. This also accounts for receivers one and three in the subplot on the right, but here receivers two and four are not so nicely separated. Additionally their distance is smaller than 0.5λ. This leads to stronger coupling between the receiving elements of receivers two and four. For the optimization, this means that

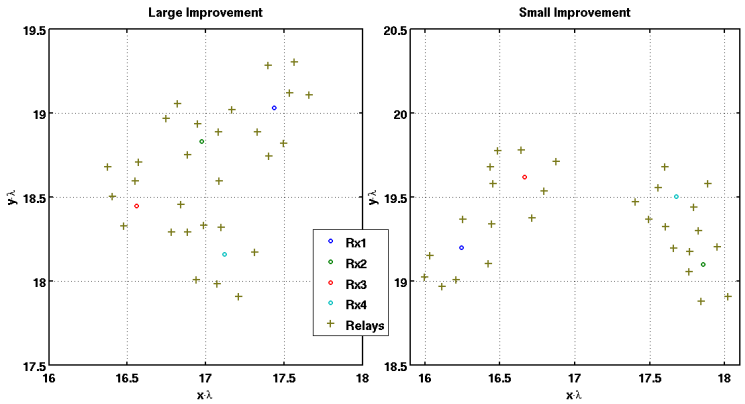

Figure 5.15: Two different antenna placings, the left leads to a big improvement; the right to a small improvement.

if one receiver and its relays are optimized their coupling might diminish the rate of the other receiver severely. This effect can be seen as an additional interferer. Any poor channel realization can lead to a case in which the second receiver rate cannot be optimized significantly.

5.6 TDMA - Combination

We assess the combination of our optimization method with currently existing interference-avoiding methods. As seen in the previous sections, the number of required relays for reducing interference grows with the number of users in the the system. For large systems with hundreds of users, the required number of relays would become extremely large, hence the optimization very complex. Therefore, a combination of our strategy with the TDMA method is one way to reduce the number of users in a single time slot, therefore reducing the number of required relays.

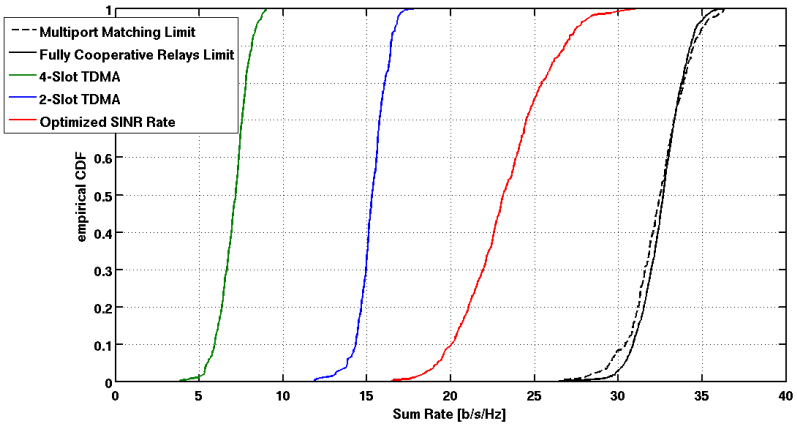

Figure 5.16: Comparison of different slot TDMA approaches.

Using two-slot TDMA, reduces the number of users per slot from four to two. Therefore, the results from Figure 5.13 can be used to compare them to TDMA applied on the results from Figure 4.13. The combination of TDMA and the optimization introduced in this thesis lead additionally to halving the problem size, therefore yielding results closer to the (corresponding) optimum from 2-slot TDMA than from the pure optimization.

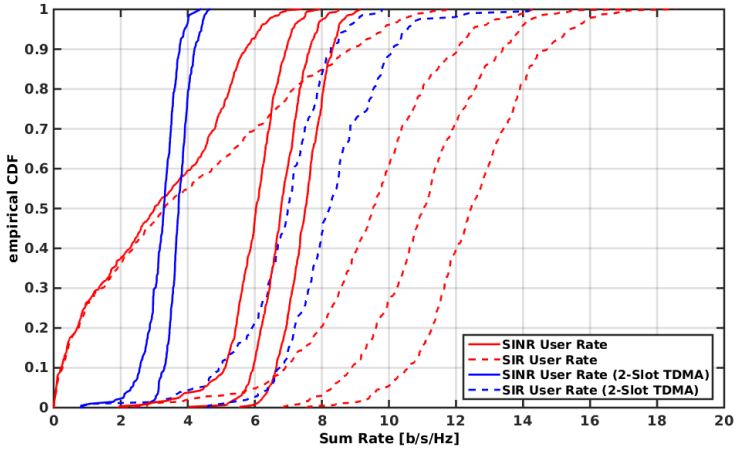

Figure 5.17: Comparison of different slot TDMA approaches for user rates.

Figure 5.16 shows in red the results of the four-user system without TDMA (or

1-slot TDMA). In blue, we show the performance of the 2-slot TDMA approach applied on a four-user system with only three relays per receiver and under the user-power constraint. In green is the performance of a 4-slot TDMA approach without the use of any relays under the sum-power constraint. The method introduced in this thesis without the use of TDMA still outperforms 2- and 4-slot TDMA. However, it can also be observed that the use of only three relays per user and a 2-slot TDMA approach outperforms the pure TDMA approach by approximately 8 [b/s/Hz]. Hence the combination of using passive relays and TDMA also significantly improves the performance of a system suffering from strong interference.

In Figure 5.17, we see the user rates for different TDMA approaches. In blue we see the 2-slot TDMA approach with its SINR- (solid curves) and SIR-rates (dashed curves). Although the achievable sum rate of the 2-slot TDMA approach is lower than the achievable sum rate of our introduced optimization strategy, it can be seen, that no user experiences blocking in order to improve the sum rate. Therefore the combination with TDMA is also a method to prevent blocking of users.

Chapter 6

Conclusion and Outlook

6.1 Conclusion

This thesis shows that the use of passive relays with an optimal choice of relay and matching network impedances can improve the achievable rates significantly. It was not only shown that current interference eliminating protocols are outperformed by our method, but also that any combination with methods like TDMA leads to far better results than those without using passive relays.

For the optimization of relay loads and the matching network of receivers, different solver approaches have been introduced with promising results. For the method of gradient search, we derived the partial derivatives of the achievable user rates and the achievable sum rate for any noise contribution, any spatial channel realization, and different antenna topologies. The optimization methods we introduced were further improved by the use of an adaptive step size, conjugate gradients method, and heuristic solvers. Their performance was further optimized by better choices of initial values, post-refinement of the solution, and stepwise optimization.

We compared the results of the optimization routine to receiver structures with widely spaced antennas and optimal choices of the matching network, assuming the relays to be fully cooperative receiving antennas. We repeated this for different number of passive relays, receiving antennas per user, users, relay placings, and input powers. With just one receiver antenna, we achieved rates close to ideal limits. We gave a lower bound of the required number of relays to achieve low interference links for all users in a network. This lower bound was then compared to a four-user system and evaluated. To achieve this lower bound, the noise-free rates of the systems were calculated and analyzed.

Finnaly, it was shown that, by keeping the sum of relays and receivers fixed we can find similarly good results independent of whether more receivers and less relays or less receivers and more relays were used. Hence, increasing the number of relays leads to almost the same improvements as increasing the number of receivers per user.

6.2 Future Work

This thesis looked into the improvements achievable through the use of passive relays and showed that this method is an auspicious method for diminishing interference in dense networks, but practical feasibility remains to be proven. For that, the system must be scaled to larger numbers of users and relays, and the speed of the solver must be improved to find satisfyingly good results. Therefore, different solver

approaches could be the solution. As the coupling is dependent on the distances among antennas, means of determining each antenna position must be found.

Further, an analysis of the optimal impedance values would most certainly lead to a better understanding. Investigating good choices of initial values would also potentiallly help, so that a normal gradient search routine with less initializations could be used. Correlations between impedance values and antenna placments could be found, hence again a better optimization routine with educated initial guesses could be found.

The choice of complex components at the relays (i.e. lossy relays), must be further explored, as it gives a higher degree of freedom for finding solutions. However, this also requires better performance from the optimization routine, in both speed and precision.

Finally, a real system setup for validation of the solver and the system would give certainty that the approach of eliminating interference by the use of passive relays is reasonable.

Appendix A

Lossy Passive Relays

In this chapter, the effect of lossy passive relays is explored. In the beginning, we justified the choice of considering only purely imaginary impedances at the relays, by the fact that this results in lossless relays. In the following, we will allow impedances to become complex, with a strict positive real part, i.e. $\mathbf{Z}_{\text{Rel}} = \mathbf{R}_{\text{Rel}} + j\mathbf{X}_{\text{Rel}}$ with $R_{\text{Rel}}[i] >= 0, \forall i \in [1, \cdots, N_{Rel}]$. It is obvious that the performance of this system must be strictly larger than when allowing only lossless relays, as we can set the real part to zero and therefore we would get the same result.

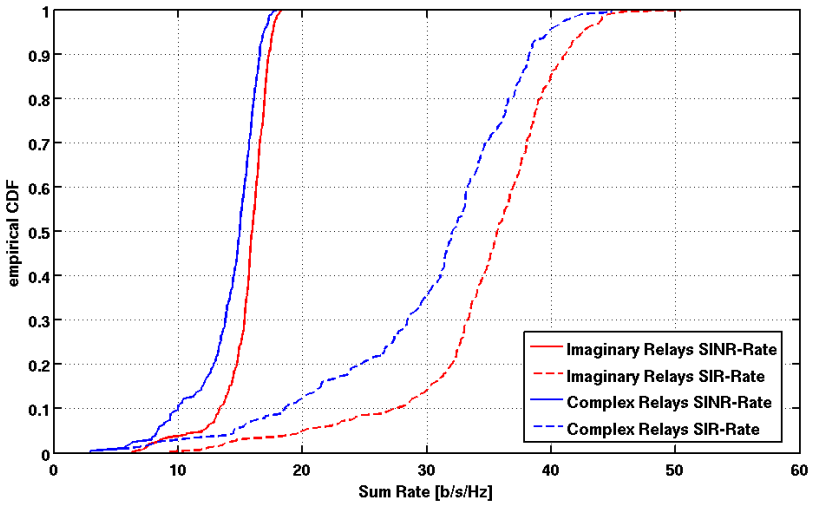

Figure A.1: Comparison of lossless and lossy relays.

Figure A.1 shows the performance of the lossless relays in red, as we know them from the previous chapters. In blue, we give the performance of the lossy relays. We see that the performance is lower than the performance of the lossless relays, which contradicts the statement above. This leads to the conclusion that the performance of the optimization routine is worse, when the degrees of freedom are larger.

Therefore, we introduce a stepwise optimization similar to the one in Section 4.4.3. At first the system is optimized for only the pure values of the relay loads. In a second step the impedances are allowed to become complex, with positive real parts — we neglect negative values, as the relays would then required a power source and noise effects would appear.

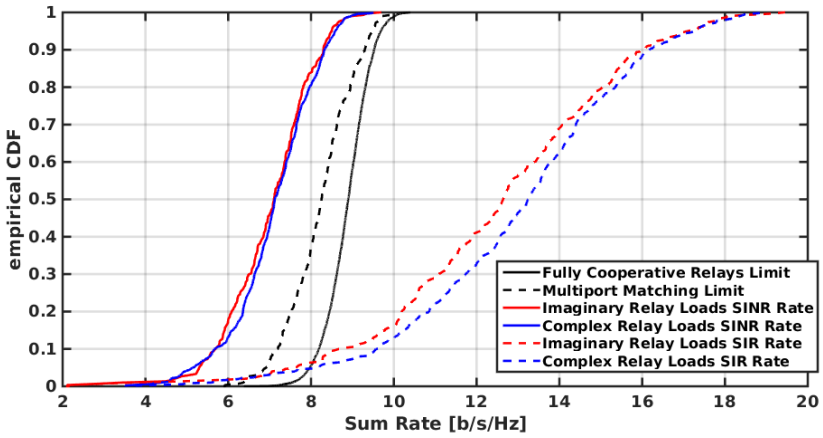

Figure A.2: Comparison of lossless and lossy relays.

Figure A.2 shows the result of this optimization for one receiver with seven relays and three interferers. We changed the settings to have a smaller problem size. By the solid lines we see, that allowing the loads to become complex (blue solid and dashed lines), improves as expected the performance. However, the improvement is not significantly larger to the lossless loads (red solid and dashed lines).

Appendix B

Alternative Description of the Receiver

As written in the Introduction of this thesis, our circuit description is based on the methods introduced in [2]. Therefore we give a similar description to that used in [2] here.

B.1 Transfer Function

To fully use this method in our context, some adaptations are made. In [2], the use of relays was not introduced. In order to use their description, we model relays as receivers with the following setting for the matching network:

$$\mathbf{Z}_{\mathrm{M11}}[N_{\mathrm{R}} \cdot N_{\mathrm{Rx}} + (1 : N_{\mathrm{Relay}})] = \mathrm{diag}\left(\mathbf{Z}_{\mathrm{Relay}}\right) \tag{B.1}$$

$$\mathbf{Z}_{\mathrm{M12}}[N_{\mathrm{R}} \cdot N_{\mathrm{Rx}} + (1 : N_{\mathrm{Relay}})] = \mathbf{Z}_{\mathrm{M21}}[N_{\mathrm{R}} \cdot N_{\mathrm{Rx}} + (1 : N_{\mathrm{Relay}})] = \mathbf{0} \tag{B.2}$$

$$\mathbf{Z}_{\mathrm{M22}}[N_{\mathrm{R}} \cdot N_{\mathrm{Rx}} + (1 : N_{\mathrm{Relay}})] = \text{undef.} \tag{B.3}$$

The equivalent input impedance matrix for the relay ports becomes

$$\mathbf{Z}_{\mathrm{inM}}[N_{\mathrm{R}} \cdot N_{\mathrm{Rx}} + (1 : N_{\mathrm{Relay}})] = \mathrm{diag}\left(\mathbf{Z}_{\mathrm{Relay}}\right). \tag{B.4}$$

B.1.1 Signal Transfer Function

Applying the circuitry transfer function from [2] to our adaptations, leads to

$$\mathbf{H}_{\mathrm{L,A}} = \frac{z_l d}{z_l + g}\mathbf{D}\mathbf{F}_{\mathrm{R}}, \quad \text{with} \tag{B.5}$$

$$\mathbf{D} = \left(c\mathbf{I} + \mathbf{Z}_{\mathrm{R}}\right)^{-1}, \tag{B.6}$$

$$\mathbf{F}_{\mathrm{R}} = \mathbf{Z}_{\mathrm{M12}}\left(\mathbf{Z}_{\mathrm{M11}} + \mathbf{Z}_{\mathrm{C}}\right)^{-1}, \quad \text{and} \tag{B.7}$$

$$\mathbf{Z}_{\mathrm{R}} = \mathbf{Z}_{\mathrm{M22}} + \mathbf{F}_{\mathrm{R}}\mathbf{Z}_{\mathrm{M12}}. \tag{B.8}$$

Note that in [2], the matching network is defined differently:$\mathbf{Z}_{\mathrm{M11}}$ and $\mathbf{Z}_{\mathrm{M22}}$ are swapped. $\mathbf{H}_{\mathrm{L,A}}$ denotes the transfer function from all the open circuit input voltages to all the voltages over the downstream circuitry loads. To get the transfer function for only receiver j, we consider only rows $[(j-1) \cdot N_{\mathrm{Rx}} + 1 : j \cdot N_{\mathrm{Rx}}]$. In the following, we denote such cases by $\mathbf{H}_{\mathrm{L},j}$ and we can write the overall transfer function as

$$\mathbf{v}^s_{\mathrm{L},j} = \mathbf{H}_{\mathrm{L},j} \cdot \mathbf{H}^{\mathrm{sp}}_j \cdot \mathbf{v}_j. \tag{B.9}$$

B.1.2 Noise Transfer Function

Similarly, the new model can be applied to noise sources. According to [3, Equation (14)], this leads to the transfer function

$$\mathbf{v}_{\mathrm{L},j}^{n} = \frac{z_l d}{z_l + g}\left(\mathbf{D}\left(\mathbf{Z}_{\mathrm{R}}\mathbf{i}_{\mathrm{LNA}} - \mathbf{v}_{\mathrm{LNA}} + \mathbf{F}_{\mathrm{R}}\mathbf{n}_{\mathrm{AR}}\right) + \frac{1}{d}\tilde{\mathbf{v}}_n\right). \tag{B.10}$$

Compared to the sources introduced in Section 2.3, the noise contribution for the LNA and the downstream noise used in this formula must be extended by the length of N_{Relay} with zeros to enable a valid matrix multiplication. As in the previous section, the index j denotes the branches of the j-th receiver, or the rows $[(j-1)\cdot N_{\mathrm{Rx}} + 1 : j \cdot N_{\mathrm{Rx}}]$ of the transfer function matrix.

B.2 Analytical Gradient

In the following, the analytical gradient will be derived. In contrast to Chapter 3, the rate is only dependent on $\mathbf{Z}_{\mathrm{M}ij}$, with $i, j \in \{1, 2\}$, as the relays were expressed by the matching network written above. Therefore, similarly to [3], with the adaptations to the matching network it follows that

$$\frac{\partial r}{\partial \mathbf{Z}_{\mathrm{M},ij}} = \frac{1}{\ln(2)}\mathrm{Tr}\Bigg(\left(\mathbf{K}_s + \mathbf{K}_i + \mathbf{K}_n\right)^{-1}\left(\frac{\partial \mathbf{K}_s}{\partial \mathbf{Z}_{\mathrm{M},ij}} + \frac{\partial \mathbf{K}_i}{\partial \mathbf{Z}_{\mathrm{M},ij}} + \frac{\partial \mathbf{K}_n}{\partial \mathbf{Z}_{\mathrm{M},ij}}\right) - \left(\mathbf{K}_i + \mathbf{K}_n\right)^{-1}\left(\frac{\partial \mathbf{K}_i}{\partial \mathbf{Z}_{\mathrm{M},ij}} + \frac{\partial \mathbf{K}_n}{\partial \mathbf{Z}_{\mathrm{M},ij}}\right)\Bigg). \tag{B.11}$$

The derivations of the rate with no interference can be found in [3]. In the following, we adapt it to the needs of this thesis. To get the gradient of the interference, the sum over all interferer is taken, as in Section 2.2.6.

For notational convenience, we define the following

$$\begin{aligned} \mathbf{G} &= \mathbf{H}_j^{\mathrm{sp}}\mathrm{J}[\mathbf{v}_j\mathbf{v}_j^H]{\mathbf{H}_j^{\mathrm{sp}}}^H, \quad \text{and} \\ \mathbf{P}_j &= \mathbf{F}_R\mathbf{G}\mathbf{F}_R^H. \end{aligned} \tag{B.12}$$

The covariance matrix of the desired signal and interference at the receiver is

$$\mathbf{K}_{\mathrm{s}} = \left|\frac{z_l d}{z_l + g}\right|^2 \mathbf{D}\mathbf{P}_j\mathbf{D}^H, \quad \text{and} \tag{B.13}$$

$$\mathbf{K}_{\mathrm{i}} = \left|\frac{z_l d}{z_l + g}\right|^2 \mathbf{D}\sum_{i=0, i\neq j}^{N_{\mathrm{User}}-1}\mathbf{P}_i\mathbf{D}^H. \tag{B.14}$$

The covariance matrix of the noise voltages $\mathbf{v}_{\mathrm{L},j}^{n}$ is given as

$$\mathbf{K}_n = \mathrm{J}[\mathbf{v}_{\mathrm{L},j}^{n}{\mathbf{v}_{\mathrm{L},j}^{n}}^H] = \left|\frac{z_l d}{z_l + g}\right|^2 \mathbf{D}\mathbf{\Phi}\mathbf{D}^H, \tag{B.15}$$

with

$$\mathbf{\Phi} = \overbrace{\beta\left(\mathbf{Z}_R\mathbf{Z}_R^H - 2R_N\Re\{\rho^*\mathbf{Z}_R\} + R_N^2\mathbf{I}_M\right)}^{\text{LNA noise}} + \overbrace{\mathbf{F}_R\mathbf{R}_{\mathrm{na}}\mathbf{F}_R^H}^{\text{Ant. noise}} + \underbrace{\frac{1}{|d|^2}\mathbf{D}^{-1}\psi\mathbf{I}_{N_{\mathrm{Rx}}}\mathbf{D}^{-H}}_{\text{Downstream noise}}. \tag{B.16}$$

To get the gradient of the achievable rate, we proceed as in [3], namely by the LNA in (B.16). Additionally, we introduce for symmetric matrices the unit-differential matrix $\mathbf{S}_{ij}$, and all-zeros matrix except for the two elements in i-th row and j-th column and j-th row and i-th column, which are equal to $1i$ (hence $\mathbf{S}_{ij} = \mathbf{J}_{ij} + \mathbf{J}_{ji}$, if $j \neq i$, else $\mathbf{S}_{ij} = \mathbf{J}_{ij}$). We start by the first term $\beta\mathbf{T}_1 = \beta\mathbf{Z}_R\mathbf{Z}_R^H$.

$$\begin{aligned}
\frac{\partial \mathbf{T}_1}{\partial \mathbf{Z}_{\mathrm{M22},ij}} &= \mathbf{S}_{ij}\mathbf{Z}_R^H + \mathbf{Z}_R(\mathbf{S}_{ij}) \\
\frac{\partial \mathbf{T}_1}{\partial \mathbf{Z}_{\mathrm{M12},ij}} &= (\mathbf{J}_{ij}\mathbf{F}_R^T + \mathbf{F}_R\mathbf{J}_{ij}^T)\mathbf{Z}_R^H + \mathbf{Z}_R(\mathbf{J}_{ij}\mathbf{F}_R^H + \mathbf{Z}_{M11}\mathbf{B}_1^H\mathbf{J}_{ij}^T) \\
\frac{\partial \mathbf{T}_1}{\partial \mathbf{Z}_{\mathrm{M11},ij}} &= \mathbf{F}_R(-\mathbf{S}_{ij})\mathbf{F}_R^T\mathbf{Z}_R^H + \mathbf{Z}_R\mathbf{Z}_{M12}\mathbf{B}_1^H(\mathbf{S}_{ij})\mathbf{F}_R^H, \qquad \text{(B.17)}
\end{aligned}$$

where we define the matrix $\mathbf{B}_1 = (\mathbf{Z}_{M11}+\mathbf{Z}_{\mathrm{CR}})^{-1}$. Since both matrices $\mathbf{Z}_{M11}$ and $\mathbf{Z}_{\mathrm{CR}}$ are symmetric, $\mathbf{B}_1$ is also symmetric.

In the second term of the LNA noise contribution $-\beta R_N\mathbf{T}_2 = -\beta R_N(\rho^*\mathbf{Z}_R + \rho\mathbf{Z}_R^*)$ the derivatives are

$$\begin{aligned}
\frac{\partial \mathbf{T}_2}{\partial \mathbf{Z}_{M22,ij}} &= \rho^*\mathbf{S}_{ij} + \rho(-\mathbf{S}_{ij}) \\
\frac{\partial \mathbf{T}_2}{\partial \mathbf{Z}_{M12,ij}} &= \rho^*(\mathbf{J}_{ij}\mathbf{F}_R^T + \mathbf{F}_R\mathbf{J}_{ij}^T) + \rho(\mathbf{J}_{ij}\mathbf{F}_R^H + \mathbf{F}_R^*\mathbf{J}_{ij}^T) \\
\frac{\partial \mathbf{T}_2}{\partial \mathbf{Z}_{M11},ij} &= \rho^*\mathbf{F}_R(-\mathbf{S}_{ij})\mathbf{F}_R^T + \rho\mathbf{Z}_{M12}\mathbf{B}_1^H(\mathbf{S}_{ij})\mathbf{F}_R^H. \qquad \text{(B.18)}
\end{aligned}$$

For the downstream noise components $\frac{\psi}{|d|^2}\mathbf{T}_3 = \frac{\psi}{|d|^2}\mathbf{D}^{-1}\mathbf{I}_M\mathbf{D}^{-H}$ the derivatives become

$$\begin{aligned}
\frac{\partial \mathbf{T}_3}{\partial \mathbf{Z}_{M22,ij}} &= \mathbf{S}_{ij}(c^*\mathbf{I}_M + \mathbf{Z}_R^H) + (c\mathbf{I}_M + \mathbf{Z}_R)(-\mathbf{S}_{ij}) \\
\frac{\partial \mathbf{T}_3}{\partial \mathbf{Z}_{M12,ij}} &= (\mathbf{J}_{ij}\mathbf{F}_R^T + \mathbf{F}_R\mathbf{J}_{ij}^T)(c^*\mathbf{I}_M + \mathbf{Z}_R^H) + \\
&\quad (c\mathbf{I}_M + \mathbf{Z}_R)(\mathbf{J}_{ij}\mathbf{F}_R^H + \mathbf{Z}_{M12}\mathbf{B}_1^H\mathbf{J}_{ij}^T) \\
\frac{\partial \mathbf{T}_3}{\partial \mathbf{Z}_{M11,ij}} &= (\mathbf{F}_R(-\mathbf{S}_{ij})\mathbf{F}_R^T)(c^*\mathbf{I}_M + \mathbf{Z}_R^H) + \\
&\quad (c\mathbf{I}_M + \mathbf{Z}_R)(\mathbf{Z}_{M12}\mathbf{B}_1^H(\mathbf{S}_{ij})\mathbf{F}_R^H). \qquad \text{(B.19)}
\end{aligned}$$

As mentioned in Chapter 3, the transfer function of the signal and the antenna noise are the same. Therefore the gradients also become the same, namely

$$\begin{aligned}
\frac{\partial \mathbf{P}}{\partial \mathbf{Z}_{M12,ij}} &= \mathbf{J}_{ij}\mathbf{B}_1\mathbf{G}\mathbf{F}_R^H + \mathbf{F}_R\mathbf{G}\mathbf{B}_1^H\mathbf{J}_{ij}^T \\
\frac{\partial \mathbf{P}}{\partial \mathbf{Z}_{M11,ij}} &= \mathbf{F}_R\left((-\mathbf{S}_{ij})\mathbf{B}_1\mathbf{G} + \mathbf{G}\mathbf{B}_1^H(\mathbf{S}_{ij})\right)\mathbf{F}_R^H. \qquad \text{(B.20)}
\end{aligned}$$

The derivative of the antenna noise is identical to (B.20), but with replacing $\mathbf{G}$ by $\mathbf{R}_{\mathrm{na}}$. With the derivatives given above, the gradient of the achievable rate can now be calculated.

Bibliography

[1] F. Rusek, D. Persson, B. K. Lau, E. Larsson, T. Marzetta, O. Edfors, and F. Tufvesson, "Scaling up mimo: Opportunities and challenges with very large arrays," *Signal Processing Magazine, IEEE*, vol. 30, pp. 40–60, Jan 2013.

[2] M. Ivrlac and J. Nossek, "Toward a circuit theory of communication," *Circuits and Systems I: Regular Papers, IEEE Transactions on*, vol. 57, pp. 1663–1683, July 2010.

[3] Y. Hassan and A. Wittneben, "Rate maximization in coupled mimo systems: A generic algorithm for designing single-port matching networks," in *Wireless Communications and Networking Conference (WCNC), 2014 IEEE*, pp. 1287–1292, April 2014.

[4] S. Berger and A. Wittneben, "Cooperative distributed multiuser mmse relaying in wireless ad-hoc networks," in *Signals, Systems and Computers, 2005. Conference Record of the Thirty-Ninth Asilomar Conference on*, pp. 1072–1076, October 2005.

[5] R. Bains, R. R. Müller, and S. Members, "Using parasitic elements for implementing the rotating antenna for mimo receivers," *IEEE Trans. on Wireless Communications*, pp. 4522–4533, 2008.

[6] B. K. Lau and J. Andersen, "Simple and efficient decoupling of compact arrays with parasitic scatterers," *Antennas and Propagation, IEEE Transactions on*, vol. 60, pp. 464–472, Feb 2012.

[7] E. Kreyszig, *Advanced Engineering Mathematics*. New York, NY, USA: John Wiley & Sons, Inc., 9th ed., 2006.

[8] Antenna Magus, "ANTENNA MAGUS - Utilities information — The leading Antenna Design Software tool. — Antenna Design. Simplified," 2015. [Online] Available: `http://www.antennamagus.com/database/utilities/tools_page.php?id=24&page=two-port-network-conversion-tool`.

[9] S. J. Orfanidis, *Electromagnetic Waves and Antennas*. ECE Department, Rutgers University, 94 Brett Road, Piscataway, NJ 08854-8058: Rutgers University, 2014. [Online]. Available: `http://www.ece.rutgers.edu/~orfanidi/ewa/`.

[10] R. Q. Twiss, "Nyquist's and Thevenin's Theorems Generalized for Nonreciprocal Linear Networks," *Journal of Applied Physics*, vol. 26, pp. 599–602, May 1955.

[11] C. Domizioli and B. Hughes, "Front-end design for compact mimo receivers: A communication theory perspective," *Communications, IEEE Transactions on*, vol. 60, pp. 2938–2949, October 2012.

[12] K. B. Petersen and M. S. Pedersen, "The Matrix Cookbook," Nov. 2012. Version 20121115.

[13] Wikipedia, "Conjugate gradient method — Wikipedia, the free encyclopedia," 2015. [Online] Available: http://en.wikipedia.org/wiki/Conjugate_gradient_method.

[14] R. Fletcher and C. M. Reeves, "Function minimization by conjugate gradients," *The Computer Journal*, vol. 7, no. 2, pp. 149–154, 1964.

[15] E. Polak and G. Ribiere, "Note sur la convergence de méthodes de directions conjuguées," *ESAIM: Mathematical Modelling and Numerical Analysis - Modélisation Mathématique et Analyse Numérique*, vol. 3, no. R1, pp. 35–43, 1969.

[16] S. Kirkpatrick, C. D. Gelatt, and M. P. Vecchi, "Optimization by simulated annealing," *SCIENCE*, vol. 220, no. 4598, pp. 671–680, 1983.

[17] The MathWorks, Inc., "How Simulated Annealing Works - MATLAB & Simulink - MathWorks Schweiz," 2015. [Online] Available: http://ch.mathworks.com/help/gads/how-simulated-annealing-works.html.

[18] The MathWorks, Inc., "How GlobalSearch and MultiStart Work - MATLAB & Simulink - MathWorks Schweiz," 2015. [Online] Available: http://ch.mathworks.com/help/gads/how-globalsearch-and-multistart-work.html#bsfjle9.